Chemistry Europe
European Chemical Societies Publishing

WILEY VCH

Excellence in Chemistry Research

Announcing our new flagship journal

- Gold Open Access
- Publishing charges waived
- Preprints welcome
- Edited by active scientists

Meet the Editors of *ChemistryEurope*

Luisa De Cola
Università degli Studi di Milano Statale, Italy

Ive Hermans
University of Wisconsin-Madison, USA

Ken Tanaka
Tokyo Institute of Technology, Japan

Chemistry–A European Journal
Research Article
doi.org/10.1002/chem.202300291
Chemistry Europe
European Chemical Societies Publishing
www.chemeurj.org

Chiral Diketopyrrolo[3,4-*c*]pyrrole-1,2,3-1*H*-triazole Dyes with Highly Tuneable Properties in Solution and Thin Films

Gianluigi Albano,[a] Francesco Zinna,[b] Andrea Taddeucci,[b, c] Maria Annunziata M. Capozzi,[a] Gennaro Pescitelli,[b] Angela Punzi,*[a] Lorenzo Di Bari,*[b] and Gianluca M. Farinola[a]

Abstract: We have studied the impact of achiral substituents on the chiral supramolecular architectures of diketopyrrolo[3,4-*c*]pyrrole-1,2,3-1*H*-triazole (DPP) dyes. We decorated the same chiral DPP motif with substituent groups on the nitrogen atoms of the lactam moiety: the hydrophobic *n*-octyl alkyl chain, the hydrophilic tri(ethylene glycol) (TEG) chain and the thermo-cleavable *tert*-butoxycarbonyl (*t*-Boc) carbamate group. In spite of having identical conjugated chromophore and chiral appendages, in aggregated form the three dyes displayed profoundly different optical, chiroptical, electrochemical and thermal features. ECD measurements revealed differences in the aggregation modes, which would be inaccessible by most other techniques. We found strong chiroptical features, which would have major implications in the context of chiral organic opto-electronics and in the development of other highly innovative technological applications.

Introduction

The extraordinary growth and development of organic π-conjugated compounds during the past 20 years is due to their wide use as semiconducting active layers in optoelectronic devices,[1] as well as to their technological applications as stimuli-responsive smart materials and metamaterials.[2] Among other positive aspects, the strength of π-conjugated systems resides in controlling their crucial physicochemical parameters (and so on) by tailoring their molecular structure.[3] Not only one can alter the chromophores themselves through their conjugation extension (impacting absorption and emission spectra or HOMO-LUMO gap), but also their solid state organization, with fallout for example on charge transfer. All hierarchical levels, from the first-order supramolecular arrangement[4] up to the mesoscopic scale[5] can be affected. On the other hand, processing conditions during thin film preparation (temperature, solvent, concentration, deposition and post deposition techniques, etc.) may lead to different polymorphs due to competing aggregation pathways (e.g., kinetic vs. thermodynamic states) featuring different optoelectronic properties.[6]

Chirality in π-conjugated backbones[7] can be simply achieved by introducing stereodefined substituents and can lead to the formation of first-order supramolecular chiral architectures (e.g., helices, spirals or chiral sheets)[8] but also to larger scale chiral morphologies (e.g., helical fibres, twisted ribbons and other chiral nano/mesoscopic arrangements).[9] A solid state organization with consistently repeating twist prevents randomly disordered as well as parallel stacks of adjacent π-conjugated units, which is desirable in order to ensure longer exciton lifetime[10] and reduce aggregation-induced fluorescence quenching.[11] Chiral organic π-conjugated materials allowed for the development of unique technological applications, as circularly polarized organic field-effect transistors (CP-OFETs),[12] circularly polarized organic light-emitting diodes (CP-OLEDs),[13] analytical (electro)chemical sensors,[14] and other highly specialized optoelectronic devices, stimuli-responsive smart materials and metamaterials in optical information storage and processing,[15] enantiopure chiral molecular magnets,[16] chirality-induced spin selectivity (CISS),[17] and many more.

Furthermore, chirality opens the avenue of elucidating aggregation with electronic circular dichroism (ECD), accessing information about supramolecular organization at the nanometre scale[18] and revealing multiple aggregation modes and local polymorphisms which would appear indistinguishable to standard optical methods,[6] and recognizing differential CP light absorption of thin films.[19]

Circularly polarized luminescence (CPL) is used for elucidating structural properties in electronic excited states, providing

[a] Dr. G. Albano, Prof. M. A. M. Capozzi, Prof. A. Punzi, Prof. G. M. Farinola
Dipartimento di Chimica
Università degli Studi di Bari Aldo Moro
Via Edoardo Orabona 4, 70126 Bari (Italy)
E-mail: angela.punzi@uniba.it

[b] Dr. F. Zinna, A. Taddeucci, Prof. G. Pescitelli, Prof. L. Di Bari
Dipartimento di Chimica e Chimica Industriale
Università di Pisa
Via Giuseppe Moruzzi 13, 56124 Pisa (Italy)
E-mail: lorenzo.dibari@unipi.it

[c] A. Taddeucci
Diamond Light Source, Ltd.
Chilton, Didcot OX11 0DE (United Kingdom)

Supporting information for this article is available on the WWW under https://doi.org/10.1002/chem.202300291

information often complementary to ECD,[20] but it also finds wide application in the exploration of CP production from solution and thin films of luminophores.[21]

The impact of the chromophoric core itself on the optoelectronic properties appears obvious. Similarly, one takes for granted that chiral appendages will be responsible for the chiroptical properties of molecules, aggregates and even on the devices derived from them. In our opinion, not at all trivial is that achiral moieties, which are very commonly introduced to control solubility, among other reasons, may exert a very major effect. For this reason, we took advantage of our experience on 1,4-diketo-3,6-diarylpyrrolo[3,4-*c*]pyrrole (DPP),[22] and we elaborated a highly modular system, which lends itself to study the impact of the achiral substituents on aggregation and on chiroptical properties.

The 1,4-diketo-3,6-diarylpyrrolo[3,4-c]pyrrole (DPP) dyes are a class of organic π-conjugated compounds with excellent thermal and photo stability:[23] long used as high-performance industrial pigments in paints, varnishes and plastics,[24] more recently they have been widely explored as useful building blocks in the synthesis of functional and smart materials with very appealing applications, including: fluorescent probes in sensing and bio-imaging,[25] two-photon-absorbing materials,[26] semiconducting active layers in optoelectronic devices such as organic field-effect transistors (OFETs)[27] and organic light-emitting diodes (OLEDs),[28] organic photovoltaic materials,[29] and so on. The DPP unit is a planar bicyclic scaffold containing two strong electron-withdrawing lactam moieties that can be easily functionalized by palladium-catalyzed coupling reactions on the (hetero)aryl groups at positions 3 and 6 or by nucleophilic substitution reactions on the nitrogen atoms under basic conditions. Despite these easy synthetic strategies for structural modification, the development of chiral DPP-based compounds functionalized with enantiopure groups is still quite limited to date. DPP derivatives bearing helicene,[30] binaphthyl,[31] and pyrido-fused myrtanyl[32] units on the terminal positions of the π-conjugated backbone have been investigated in solution and thin films by optical and chiroptical spectroscopies. Moreover, some DPP dyes N-substituted on the lactam moieties with chiral alkyl branched chains have been also reported.[22,33]

In this work, we investigate chiral DPP-based compounds functionalized with enantiopure alkyl branched chains on the terminal positions of the π-conjugated backbone, that is, diketopyrrolo[3,4-*c*]pyrrole-1,2,3-1*H*-triazole dyes **1**–**3** (Figure 1) bearing two β-citronellyl chiral units attached to the lateral 1,2,3-1*H*-triazole rings, characterized by the presence of substituent groups of different lengths and polarities on the nitrogen atoms of lactam moieties: i) the hydrophobic *n*-octyl alkyl chain in the case of dye **1**; ii) the hydrophilic tri(ethylene glycol) (TEG) chain in the case of dye **2**; iii) the thermo-cleavable *tert*-butoxycarbonyl (*t*-Boc) carbamate group in the case of dye **3** (Figure 1). The choice of β-citronellyl unit as the chiral appendage is due to multiple reasons. First, it can be easily introduced by using β-citronellol as the starting material, which is available in nature in both enantiopure forms: (*S*)-(−)-β-citronellol is typically extracted from citronella oils, while (*R*)-(+)-β-citronellol can be found in rose oils and pelargonium geranium.[34] Second, it transfers its molecular asymmetry (stereogenic centre at the C3 of the branched chain) to the entire system (chirality at supramolecular and mesoscopic scale) mainly through dispersion forces and steric effects. The enantiopure terpene units are anchored on the terminal positions of the π-conjugated backbone through 1,2,3-1*H*-

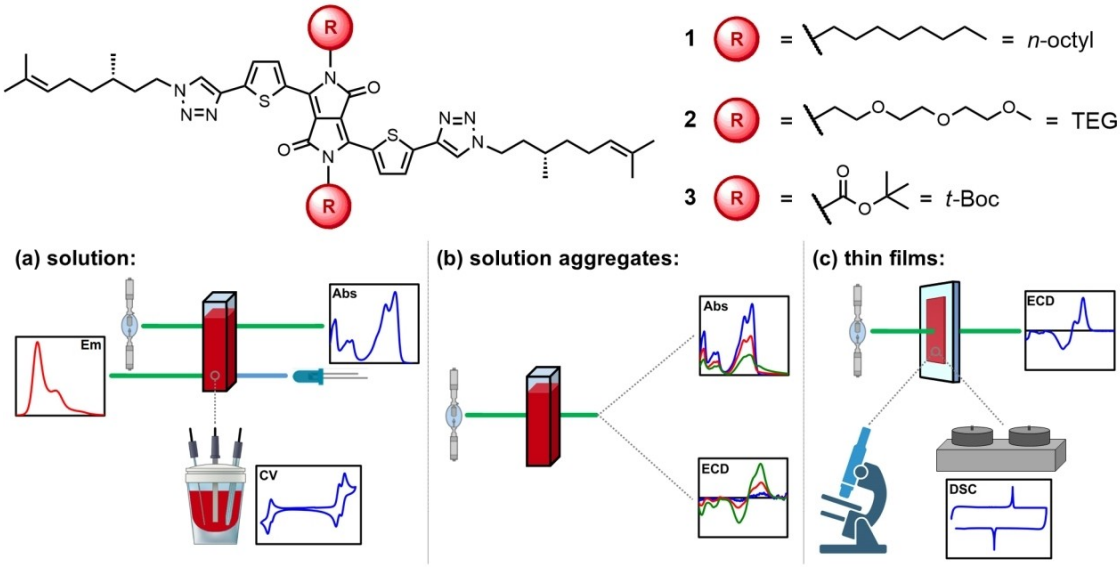

Figure 1. Scope of the work: three new chiral diketopyrrolo[3,4-*c*]pyrrole-1,2,3-1*H*-triazole dyes **1**–**3**, differing in the presence of groups of diverse lengths and polarities (*n*-octyl, TEG, *t*-Boc) on the nitrogen atoms of lactam moieties, were synthesized and characterized by several techniques: a) in solution, b) under solution aggregation and c) in thin films. The occurrence of significantly different optical, chiroptical, electrochemical and thermal features revealed the high tunability of their physico-chemical properties, mainly due to the impact of these (achiral) groups on the (chiral) supramolecular aggregation modes of the systems.

triazole units, which have been selected not only in light of their high chemical stability to acidic and basic conditions, as well as to reductive and oxidative environments, but also for their active participation to the solid state organization at different hierarchical levels via dipole–dipole and π-stacking interactions.[35]

The length of the π-conjugated backbone is definitely a key parameter affecting the photo-physical properties of DPP-based dyes, as well as their morphology and structural ordering;[23] at the same time, varying the length and/or functionalization of terminal aliphatic side chains as well as the N-substitution of DPP dyes by introducing groups of different steric hindrance and polarity may have large impact on their self-assembly and, in turn, on their solid-state optical and electrical features.[36] It is well known that the introduction of alkyl chains on the nitrogen atoms of lactam moieties (e.g., the *n*-octyl moiety of DPP dye **1**) results in significant improvement of the DPP solubility, as they are no longer able to form intermolecular hydrogen bonds; moreover, both the length and bulkiness of alkyl chains can strongly affect the aggregation behaviour of π-conjugated materials, thus impacting their opto-electronic properties.[37] The N-substitution of DPP dyes with hydrophilic oligoether chains (e.g., the TEG moiety of DPP dye **2**) allows an increased processability in environmentally friendly polar solvents, often ensuring strong self-assembling effects associated to improved charge-transport characteristics[38] and photovoltaic performance;[39] at the same time, the use of oligoether chains has extended the use of DPP-based π-conjugated materials in aqueous environments for biological applications.[40] Carbamates are a typical structural motif used as thermo-cleavable protecting groups of the nitrogen atoms of DPP units (e.g., the *t*-BOC moiety of DPP dye **3**): their introduction as electron-withdrawing and solubilizing moieties on the lactam rings was reported to be successfully employed in the fabrication of thin films of DPP-based organic semiconductors with improved morphological stability.[41] Besides polarity, the three selected achiral side chains significantly differ also in their steric features, which could have a relevant effect on the self-assembly process: on the one hand, the rigid and compact *t*-Boc group on DPP-triazole dye **3**, responsible for a considerable hindrance near the nitrogen atoms of the lactam moieties; on the other, the longer and more flexible *n*-octyl and TEG chains of DPP-triazole dyes **1**–**2**, ensuring an overall lower grade of steric hindrance in the proximity of the nitrogen atoms of lactam moieties.

By keeping both the π-conjugated backbone and the alkyl chiral units unchanged, in this work we have investigated the effect of introducing three groups of different polarity and steric hindrance on the nitrogen atoms of lactam moieties of DPP-based dyes: interestingly, for each of them we observed the occurrence of significantly different optical, chiroptical, electrochemical and thermal features in solution and/or thin films, thus revealing high tunability in the physicochemical properties of these π-conjugated systems despite only minor structural variation. In particular, we highlighted the impact of these achiral groups on the chiral supramolecular aggregation modes of DPP-triazole dyes **1**–**3** giving special emphasis to ECD measurements, able of revealing useful information that one would not obtain by using optical spectroscopy and microscopy techniques.

Results and Discussion

The preparation of chiral DPP-triazole dyes **1**–**3** was carried out according to a three-steps synthetic procedure depicted in Scheme 1. In the first step, dibrominated DPP derivatives **4a**–**c** were treated with (trimethylsilyl)acetylene **5** to give a palladium-catalysed Sonogashira coupling: despite some differences in the experimental conditions (in particular, the Palladium species used: $Pd(OAc)_2$ for **4a**, $Pd(PPh_3)_4$ for **4b**, $Pd(PPh_3)_2Cl_2$ for **4c**), the corresponding bis-(trimethylsilyl)ethynyl DPP compounds **6a**–**c** were obtained in good yields (60–76%). The subsequent desilylation step, performed with a large excess (10 equiv.) of KF in THF/H_2O mixture, afforded the deprotected alkynes **7a**–**c** in 90–99% yields. In the last step, a CuAAC cycloaddition reaction with the enantiopure (*S*)-citronellyl azide (*S*)-**8**, in turn obtained starting from (*S*)-(+)-citronellyl bromide according to literature procedure[42] (for detail, see Supporting Information), was performed with $Cu(OAc)_2 \cdot H_2O$ as the catalyst, to give the final chiral DPP-triazole dyes **1**–**3** in satisfactorily yields (42–67%). Furthermore, we also prepared on a smaller scale the opposite enantiomer of chiral DPP-triazole dyes **1** and **2**, that is, compounds *ent*-**1** and *ent*-**2**, by CuAAC cycloaddition reaction of, respectively, **7a** and **7b** with (*R*)-citronellyl azide (*R*)-**8** (see the Supporting Information for detailed experimental procedures).

We started the characterization of the three chiral DPP-triazole dyes **1**–**3** with their optical properties in solution: the UV–vis absorption and photoluminescence emission spectra in $CHCl_3$ are depicted in Figure 2.

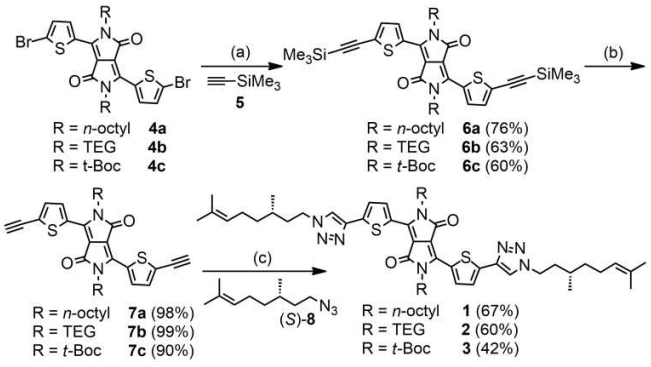

Scheme 1. Synthesis of chiral diketopyrrolo[3,4-*c*]pyrrole-1,2,3-1*H*-triazole dyes **1**–**3**. Conditions: a) for **4a**: **5** (3.0 equiv.), $Pd(OAc)_2$ (5 mol%), PPh_3 (15 mol%), CuI (5 mol%), Et_3N/CH_2Cl_2 (1:3 *v/v*), 0 °C→65 °C, 24 h; for **4b**: **5** (4.0 equiv.), $Pd(PPh_3)_4$ (5 mol%), CuI (10 mol%), Et_3N, 60 °C, 4 h; for **4c**: **5** (4.0 equiv.), $Pd(PPh_3)_2Cl_2$ (5 mol%), CuI (10 mol%), Et_3N, THF, 60 °C, 4 h; b) for **6a**: KF (10 equiv.), THF/H_2O (7:3 *v/v*), RT, 6 h; for **6b**: KF (10 equiv.), THF/H_2O (3:1 *v/v*), RT, 6 h; for **6c**: KF (10 equiv.), THF/H_2O (4:1 *v/v*), RT, 6 h; c) for **7a**: (*S*)-**8** (3.0 equiv.), $Cu(OAc)_2 \cdot H_2O$ (20 mol%), H_2O, 80 °C, 24 h; for **7b**: (*S*)-**8** (4.0 equiv.), $Cu(OAc)_2 \cdot H_2O$ (20 mol%), H_2O, 80 °C, 24 h; for **7c**: (*S*)-**8** (6.0 equiv.), NaAsc (0.6 equiv.), $Cu(OAc)_2 \cdot H_2O$ (35 mol%), THF/H_2O (1:1 *v/v*), 65 °C, 4 h.

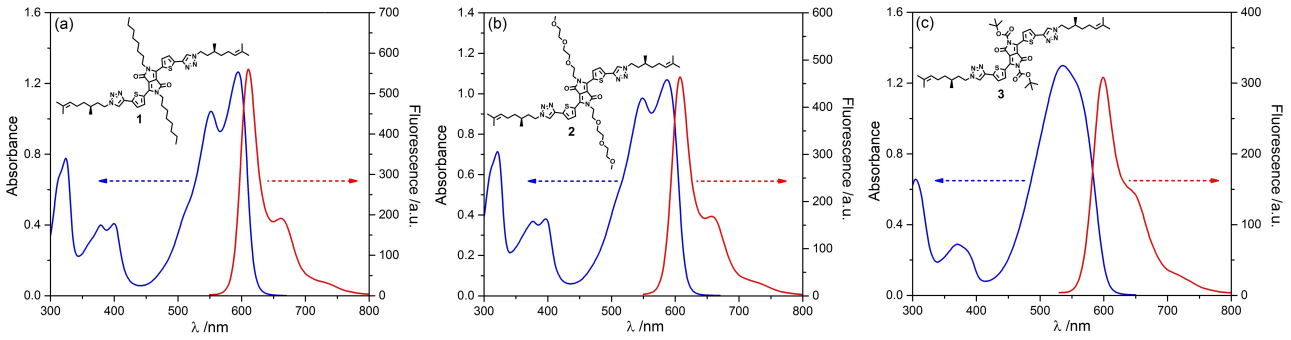

Figure 2. UV–vis absorption (blue line) and photoluminescence emission (red line) spectra in $CHCl_3$ of: a) *n*-octyl-functionalized DPP-triazole **1**, b) TEG-functionalized DPP-triazole **2** and c) *t*-Boc-functionalized DPP-triazole **3**. For UV–vis absorption measurements: cell length 2 mm; sample concentration 10^{-4} M. For photoluminescence emission measurements: cell length 1 cm; sample concentration 10^{-6} M, excitation wavelength 550 nm (for dyes **1** and **2**) or 530 nm (for dye **3**).

In the case of *n*-octyl-functionalized DPP dye **1**, the UV–vis absorption spectrum (Figure 2a, blue line) showed a broad band between 450 nm and 650 nm, with maximum at 594 nm ($\varepsilon = 6.39 \times 10^4\ M^{-1}\,cm^{-1}$), mainly attributable to a local $\pi \rightarrow \pi^*$ transition[22] rather than to an intramolecular charge-transfer (CT) transition from the thiophene rings to the DPP moiety,[43] and a more structured band at higher energy due to a second different $\pi \rightarrow \pi^*$ transition of the π-conjugated backbone, with maximum at 397 nm ($\varepsilon = 2.15 \times 10^4\ M^{-1}\,cm^{-1}$). The fluorescence emission spectrum of **1** (Figure 2a, red line) revealed a quite specular profile to the main UV–vis absorption band, with maximum emission at 611 nm; despite a modest Stokes shift (only 17 nm), it showed a fluorescence quantum yield ϕ of 34%. Interestingly, moving from a hydrophobic alkyl chain to a hydrophilic oligoether chain we did not observe significant changes in the optical properties: the UV–vis absorption of TEG-functionalized DPP-triazole **2** (Figure 2b, blue line) showed maximum absorbance at 587 nm ($\varepsilon = 4.74 \times 10^4\ M^{-1}\,cm^{-1}$) and 394 nm ($\varepsilon = 1.31 \times 10^4\ M^{-1}\,cm^{-1}$), while the photoluminescence spectrum of **2** (Figure 2b, red line) revealed maximum emission at 608 nm; moreover, only a very modest increase in the Stokes shift (i.e., 21 nm) and in the fluorescence quantum yield ϕ (i.e., 37%) was found. On the contrary, the introduction of a *t*-Boc carbamate group caused relevant differences in the optical features of DPP-triazole π-conjugated chromophore. The UV–vis absorption spectrum of **3** (Figure 2c, blue line) was blue-shifted by about 50 nm compared to dyes **1** and **2** and characterized by a less resolved vibronic structure, with the main broad band between 400 nm and 600 nm centred at 536 nm ($\varepsilon = 6.69 \times 10^4\ M^{-1}\,cm^{-1}$) and a further band at 371 nm ($\varepsilon = 1.76 \times 10^4\ M^{-1}\,cm^{-1}$). The fluorescence spectrum of **3** (Figure 2c, red line) showed only a modest blue shift, with maximum emission at 599 nm, thus resulting in a significant increase of the Stokes shift (63 nm) compared to dyes **1** and **2**. However, at the same time, the fluorescence quantum yield ϕ was significantly lower (only 20%). The UV–vis absorption and photoluminescence spectra of chiral DPP-triazole dyes **1**–**3** were also measured in THF (Figure S1 in the Supporting Information) and toluene (Figure S2): only minor differences with respect to $CHCl_3$ solution were found, suggesting that the optical properties of these π-conjugated materials are not affected by solvatochromic effects, at least in the explored solvents. The optical band gaps (E_g^{opt}) of compounds **1**–**3**, estimated from the absorption onset (λ_{onset}) in the UV–vis spectra (obtained from the intercept of the red-side slope of low energy absorption band with the wavelength axis), were all found very similar in the three investigated solvents (i.e., $CHCl_3$, THF and toluene), ranging between 2.00 and 2.05 eV.

All the relevant data of the optical properties of chiral DPP-triazole dyes **1**–**3** in $CHCl_3$, THF and toluene solution are summarized in Table 1, while all the plots for the determination of molar extinction coefficients ε (Figures S3–S11), fluorescence quantum yields ϕ (Figures S12–S20) and UV–vis absorption onset λ_{onset} (Figures S21–S23) can be found in the Supporting Information.

The three different groups attached on the nitrogen atoms of lactam moieties of chiral DPP-triazole dyes **1**–**3** were anticipated to have some impact on their electrochemical properties in solution, which were investigated by means of cyclic voltammetry (Figure 3). A gradual increase in the oxidation potential E_{ox} values was observed moving from the hydrophobic *n*-octyl alkyl chain ($E_{ox} = 0.28$ V) to the hydrophilic TEG chain ($E_{ox} = 0.38$ V) and then to the *t*-Boc group ($E_{ox} = 0.52$), while a specular decrease was observed in the case of reduction potential E_{red} values (from −1.61 V of TEG-functionalized DPP dye **2** to −1.45 V of *t*-Boc-functionalized DPP dye **3**). A similar trend was also found for the energy levels of both the frontier orbitals (estimated from electrochemical data by empirical equations, Table 2), which could be attributed to the different electronic properties of the groups on the nitrogen atoms: moving from the apolar and electron-donating *n*-octyl group of **1** to the moderately polar oligoether chain of **2** up to the strongly polar and electron-withdrawing *t*-Boc group of **3**, the HOMO energy decreased from −5.38 eV to −5.62 eV, while the LUMO one decreased from −3.38 eV to −3.65 eV. However, it is worth emphasizing that the electrochemical band gaps (E_g^{el}) of chiral DPP-triazole dyes were found very similar for all of them, with values ranging between 1.97 and 1.99 eV, and at the same time consistent with the aforementioned optical band gaps E_g^{opt} (ca. 2.00–2.05 eV, Table 1).

Table 1. Optical properties of chiral DPP-triazole dyes in $CHCl_3$, THF and toluene solution.

DPP-triazole dye	Solvent	λ_{abs}^{max} [nm][a]	ε^{max} [10^4 M^{-1} cm^{-1}][b]	λ_{em}^{max} [nm][c]	ϕ [%][d]	λ_{onset} [nm][e]	Stokes shift [nm][f]	E_g^{opt} [eV][g]
1	$CHCl_3$	594	6.39	611	34	620	17	2.00
		397	2.15				214	
	THF	594	5.33	608	32	618	14	2.01
		399	2.35				209	
	toluene	597	7.57	612	33	621	15	2.00
		398	2.45				214	
2	$CHCl_3$	587	4.74	608	37	617	21	2.01
		394	1.31				214	
	THF	589	5.09	605	35	615	16	2.02
		397	1.31				208	
	toluene	592	4.65	609	35	619	17	2.00
		396	1.64				213	
3	$CHCl_3$	536	6.69	599	20	604	63	2.05
		371	1.76				228	
	THF	537	6.74	596	21	604	59	2.05
		375	1.09				221	
	toluene	538	6.36	600	21	606	62	2.05
		375	1.78				225	

[a] Wavelength of maximum light absorbance. [b] Molar extinction coefficient corresponding to λ_{abs}^{max}. [c] Wavelength of maximum light emission (at λ_{ex} = 550 nm for DPP-octyl and DPP-TEG, 530 nm for DPP-*t*BOC). [d] Fluorescence quantum yield determined by the relative method using rhodamine B in absolute ethanol as the reference. [e] Onset wavelength determined from the intercept of the red-side slope of the absorbance main band with the wavelength axis. [f] Stokes shift defined as $\lambda_{em}^{max}-\lambda_{abs}^{max}$. [g] Optical band gap evaluated as $E_g^{opt}=1240/\lambda_{onset}$.

Table 2. Electrochemical properties of chiral DPP-triazole dyes in dichloromethane solution.

DPP-triazole dye	E_{ox} [V][a]	HOMO [eV][b]	E_{red} [V][c]	LUMO [eV][d]	E_g^{el} [eV][e]
1	0.28	−5.38	–	−3.38[f]	–
2	0.38	−5.48	−1.61	−3.49	1.99
3	0.52	−5.62	−1.45	−3.65	1.97

[a] Oxidation potential calculated as the average value between the oxidation potential peak and the related reverse one of the DPP dye vs. ferrocene/ferrocenium (Fc/Fc^+) reference. [b] HOMO energy level estimated by the empirical equation $HOMO=-e(E_{ox}+5.1\ V)$. [c] Reduction potential calculated as the average value between the reduction potential peak and the related reverse one of the DPP dye vs. ferrocene/ferrocenium (Fc/Fc^+) reference. [d] LUMO energy level estimated by the empirical equation $LUMO=-e(E_{red}+5.1\ V)$. [e] Electrochemical band gap evaluated as $E_g^{el}=e(E_{ox}-E_{red})$. [f] For DPP **1**, LUMO energy level was estimated as LUMO=HOMO$+E_g^{opt}$, where E_g^{opt} is the optical band gap in $CHCl_3$.

Moving on the characterization of chiral DPP-triazole dyes **1**–**3** under condition of solution aggregation, induced by the use of solvent mixtures consisting of a good solvent and a poor solvent (i.e., $CHCl_3$/MeOH or THF/H_2O) in different ratio, we found a more evident impact of the side chains of the lactam moieties on the optical and chiroptical properties of these systems. Concerning the UV–vis absorption spectra (Figures S24 and S25), in the case of *n*-octyl-functionalized DPP-triazole dye **1** we observed for both $CHCl_3$/MeOH and THF/H_2O mixtures, by increasing the amount of the poor solvent, a gradual hypochromism and the formation of a shoulder for the band at lower energy (the so-called *aggregation band*),[44] which is an important indication of supramolecular self-assembly. For TEG- and *t*-Boc-functionalized DPP **2** and **3**, the same phenomena were only observed in the case of THF/H_2O mixture, while in $CHCl_3$/MeOH no evidence of supramolecular aggregation was found, with the same spectral profiles maintained up to 99% MeOH. The different behaviour in the optical properties can be explained in terms of solubility: for DPP **1**, bearing the apolar hydrophobic *n*-octyl chain, both methanol and H_2O are poor enough solvents to induce a strong self-assembly of the π-conjugated molecules at relatively low amounts; for DPPs **2** and **3**, bearing the polar and more hydrophilic TEG and *t*-Boc groups, methanol is not able to induce supramolecular aggregation, which instead occurs by using H_2O.

However, the corresponding ECD spectra (Figure 4) provided us more information about the different aggregation modes of these conjugated compounds. Interestingly, in the case of **1** we observed the occurrence of totally different spectral profiles in the two selected solvent mixtures. In $CHCl_3$/MeOH, two highly structured negative ECD bands appeared at 85% MeOH, which increased gradually in intensity by further addition of MeOH up to 98%, where maximum dissymmetry factors g_{abs} of -2.56×10^{-2} at 620 nm and -1.70×10^{-2} at 404 nm (Figure 4a) were attained; in the same spectra, the positive ECD signals above 650 nm can presumably be attributed to differential scattering of solution aggregates. In THF/H_2O we found different yet similarly complex ECD profile, with maximum intensity at 80% H_2O, consisting of several bands including a strong positive signal centred at 653 nm ($g_{abs}=+0.21$) and a further positive band at 421 nm ($g_{abs}=+0.12$; Figure 4b). These results clearly suggested the occurrence of two different chiral aggregation modes, presumably characterized by an opposite helicity. This result is not surprising: in THF/H_2O mixtures, the formation of supramolecular aggregates is presumably affected by a strong hydrophobic effect of *n*-octyl chains caused by the use of H_2O, which forced DPP-triazole molecules to self-assemble into a different supramolecular organization, with opposite helicity with respect to $CHCl_3$/MeOH mixtures. An alternative explanation could be the direct participation of H_2O into supramolecular aggregates, through

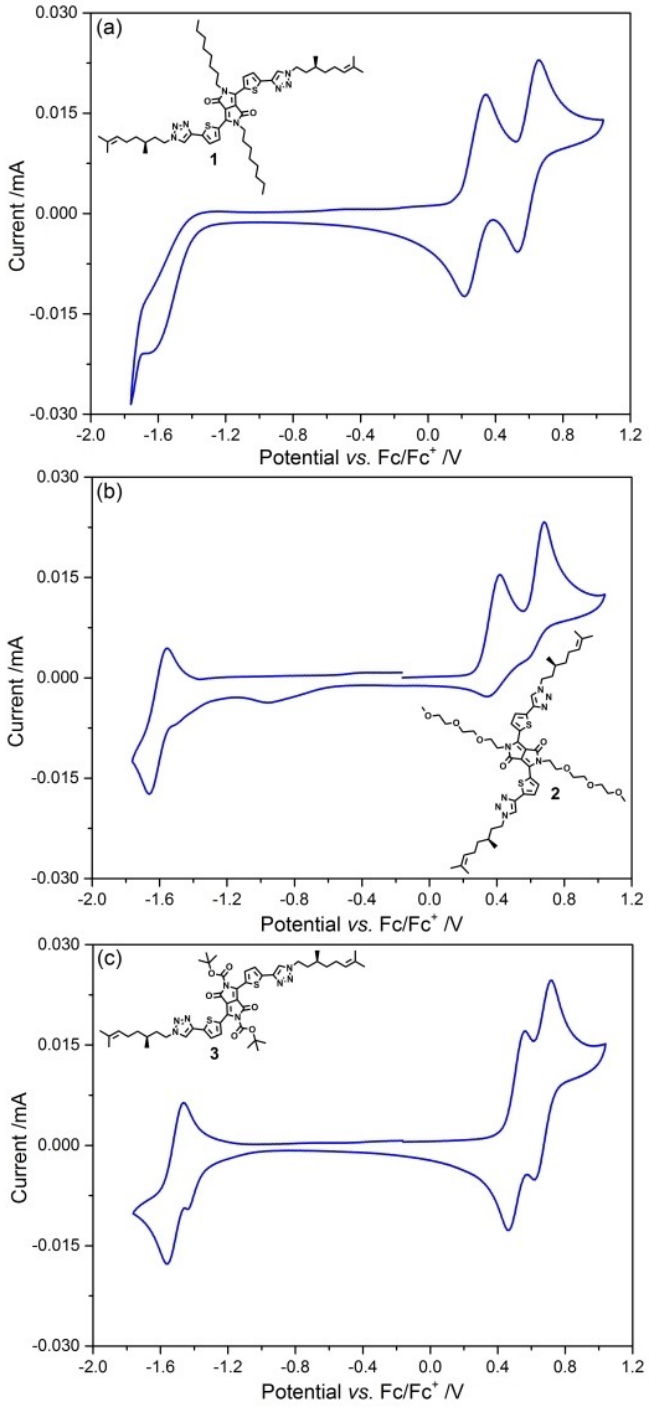

Figure 3. Cyclic voltammograms of a) *n*-octyl-functionalized DPP-triazole dye **1**, b) TEG-functionalized DPP-triazole dye **2** and c) *t*-Boc-functionalized DPP-triazole dye **3** recorded on a glassy carbon working electrode in 0.1 M *n*-Bu_4NPF_6/anhydrous CH_2Cl_2 at room temperature.

the formation of bridging bonds between two adjacent DPP-triazole molecules thanks to hydrogen bonding; in this way, a less effective stacking between adjacent π-conjugated systems could help the formation of different supramolecular aggregates, characterized by opposite helicity with respect to aggregation in $CHCl_3$/MeOH. In the case of **2**, negligible ECD signals were found in $CHCl_3$/MeOH mixtures (Figure 4c), indicating the absence of any kind of chiral supramolecular self-assembly: the perturbation exerted on the intrinsically achiral π-conjugated chromophore of DPP-triazole dye **2** by individual chiral centres of the two (*S*)-(+)-citronellyl moieties is very small in dissolved molecules. At the same time, in THF/H_2O mixtures a structured ECD signal appeared, described as an asymmetric positive exciton couplet[18d] with maximum intensity at 97% H_2O ($g_{abs} = +2.21\times10^{-2}$ at 648 nm and $g_{abs} = -1.43\times10^{-2}$ at 527 nm), suggesting the occurrence of a right-handed supramolecular aggregate held together by the twisted π-stacking of thiophene and 1*H*-triazole aromatic units with a well-defined helicity (Figure 4d).

A negligible ECD signal was found in $CHCl_3$/MeOH also in the case of **3** (Figure 4e), confirming the absence of solution aggregates already observed in the corresponding absorption spectra; a different situation occurred in THF/H_2O mixtures, where a structured ECD spectrum gradually increased in intensity by addition of the non-solvent up to 93% H_2O, consisting of a negative band at 651 nm ($g_{abs} = -1.40\times10^{-2}$), two positive bands at 567 and 617 nm ($g_{abs} = +5.36\times10^{-3}$) and a negative band at 501 nm ($g_{abs} = -3.33\times10^{-3}$; Figure 4f). A similar trend was also observed in the dissymmetry factor g_{abs} spectra (Figures S26 and S27), which provided a more intuitive view on the strength of chiroptical dissymmetry for the three chiral DPP-triazole dyes **1**–**3**. Therefore, despite chiral DPP-triazole dyes **1**–**3** are functionalized with the same enantiopure (*S*)-(+)-citronellyl chains, the three different achiral groups on the lactam moieties seem to have a large impact on their chiral supramolecular aggregation: in other words, the introduction of achiral side chains with different lengths and polarities in the chemical structure of these dyes, by keeping both π-conjugated backbone and enantiopure chiral moieties the same, is a simple and straightforward tool for tuning their chiroptical features. The most relevant data of both optical and chiroptical features of chiral DPP-triazole dyes **1**–**3** in conditions of maximum solution aggregation are summarized in Table S1.

The relevant impact of *n*-octyl, TEG and *t*-Boc side groups on the aggregates of chiral DPP-triazole dyes **1**–**3** is particularly glaring in the case of thin films, where we observed the occurrence of very different behaviour for each of them. The ability to recognize and control different aggregation modes in thin film samples would be definitely useful for obtaining layers of chiral π-conjugated materials with highly tuneable properties for innovative optoelectronic and other technological applications.[45] For each compound, thin films were prepared by drop casting (DC) or spin coating (SC) $CHCl_3$ solutions; all the samples showed a thickness of about 100 nm and macroscopically looked semi-transparent. The effect of two different post-deposition operations was also evaluated: solvent annealing (samples kept for 1 h in a closed chamber saturated with $CHCl_3$ vapours) and thermal annealing (samples kept for 1 h in an oven at 100 °C).

The characterization of chiral DPP-triazole dyes **1**–**3** in thin films started with the study of their optical and chiroptical features. However, it is worth emphasizing that ECD measurements in thin films require more attention than for isotropic

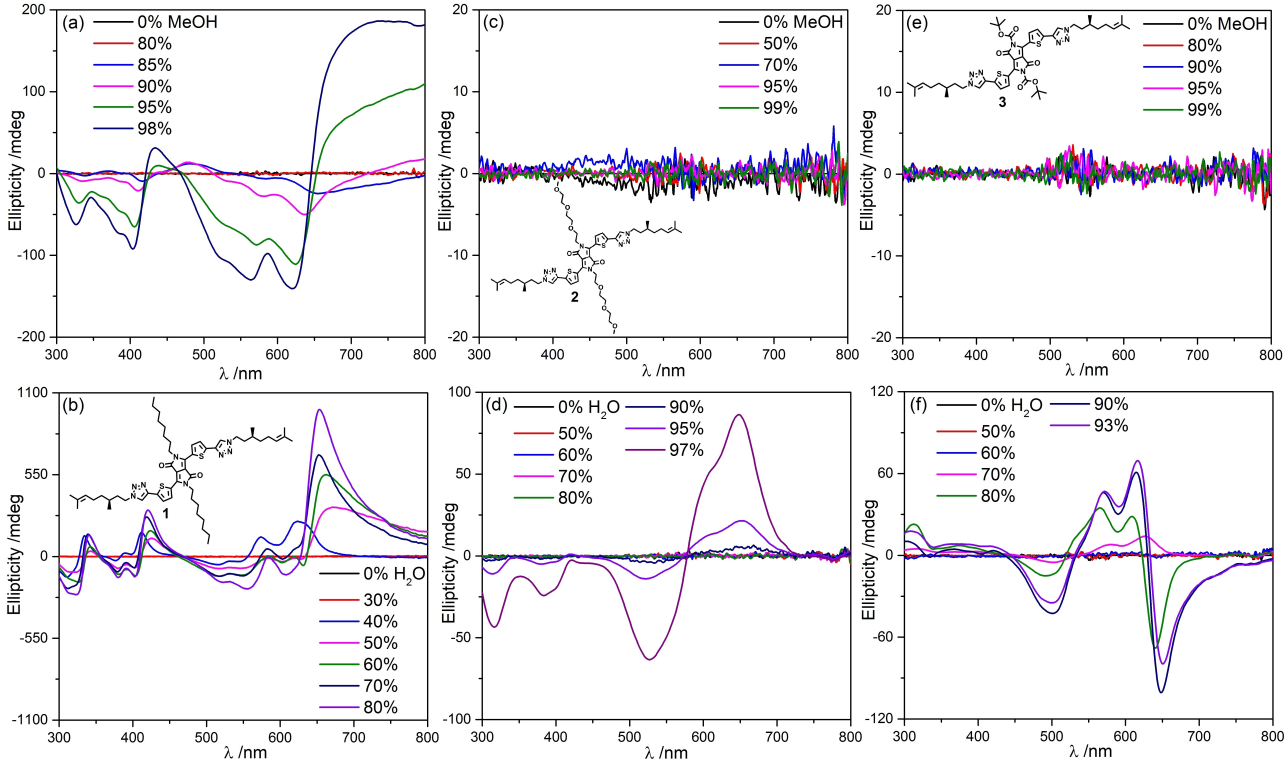

Figure 4. Chiroptical investigation of chiral DPP-triazole dyes **1–3** under conditions of solution aggregation. ECD spectra of a) *n*-octyl-functionalized DPP-triazole **1**, c) TEG-functionalized DPP-triazole **2**, e) *t*-Boc-functionalized DPP-triazole **3** in $CHCl_3$/MeOH mixtures with increasing amounts of MeOH; ECD spectra of b) *n*-octyl-functionalized DPP-triazole **1**, d) TEG-functionalized DPP-triazole **2**, f) *t*-Boc-functionalized DPP-triazole **3** in THF/H_2O mixtures with increasing amounts of H_2O. Sample concentration: 1.0×10^{-4} M.

solutions, because of the contributions of macroscopic anisotropies which can be present in the solid state, that is, linear dichroism (LD) and linear birefringence (LB).[46] In particular, the experimental ECD signal of a thin film is the sum of two main contributions: i) the conventional circular dichroism (hereafter indicated simply as CD) which is invariant upon sample orientation, which manifests itself through the rotatory strength and it is related to molecular and supramolecular chirality; ii) the LDLB arising from the combined effect of misaligned (neither parallel nor orthogonal) linear anisotropies LD and LB, which inverts its sign by sample flipping, occurring in structures where a superior order of chiral aggregates is imparted by the surface where the sample is laid upon.[46] In other words, recognizing and quantifying CD and LDLB in the ECD spectra of thin films can provide relevant information on their solid state organization at different hierarchy levels. Other contributions of spurious nature can be considered as artifacts, as they typically provide different values when the same thin film sample is measured on different instruments; however, by repeating ECD measurements at different rotation angles around the optical axis, it is possible to exclude them.

For each thin film sample described below, the ECD was recorded for both front and back side at different rotational angles around the spectropolarimeter optical axis (Figures S28–S45), but in all the cases we found very similar spectral profiles.[46] Therefore, in the following we can safely neglect any contribution due to LDLB (as well as any artifact arising from instrumental limitations based on the polarization-modulation technique), attributing all the ECD signals to a pure CD due to the occurrence of supramolecular chiral aggregates. Interestingly, this is a quite different behaviour compared to other previously reported DPP dyes bearing chiral alkyl branched chains on the lactam moieties, where the occurrence of a large LDLB contribution was found in some cases.[22]

The spin-coated sample of *n*-octyl-functionalized chiral DPP-triazole dye **1** (**SC-1**) presented a quite complex ECD profile (Figure 5a), consisting of a series of strong positive and rather narrow bands at 638 nm ($g_{abs}=+2.86\times10^{-2}$), 411 nm ($g_{abs}=+2.21\times10^{-2}$) and 333 nm ($g_{abs}=+1.72\times10^{-2}$). Interestingly, such spectrum was found roughly similar to the solution aggregates spectrum in THF/H_2O mixtures (Figure 4b), thus suggesting the occurrence of a similar aggregation mode also in thin film. The same similarity with solution aggregates in 80% H_2O was also observed in the UV–vis absorption spectrum of **SC-1** (Figure S31), although the large bandwidth and the presence of the shoulder at low energy suggested the occurrence of stronger intermolecular interaction in the solid state. No changes in both UV–vis absorption and ECD spectra of **SC-1** were observed upon solvent annealing (Figure S32) and thermal annealing (Figure S33), and very similar spectral profiles were also observed in the case of the drop-cast sample **DC-1** (Figures S28–S30).

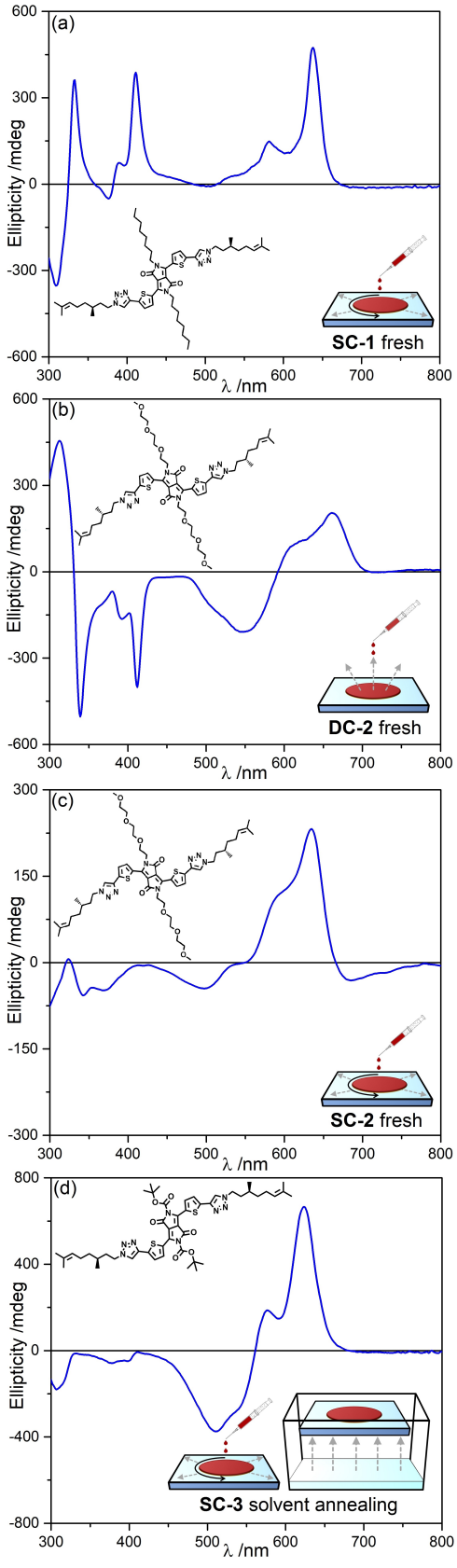

Figure 5. ECD spectra, normalized with respect to maximum absorbance, of chiral DPP-triazole dyes in thin films obtained under the most relevant experimental conditions: a) freshly prepared **SC-1** sample, b) freshly prepared **DC-2** sample, c) freshly prepared **SC-2** sample and d) **SC-3** sample after solvent annealing.

In the case of *n*-octyl-functionalized chiral DPP-triazole dye **1**, the optical and chiroptical properties in thin films seem totally independent of deposition technique and post-deposition operations. In other words, in the solid state, DPP-triazole chromophores of **1** are able to self-assemble directly into a thermodynamically stable aggregation state. The ECD spectrum of this state is apparently non-conservative in the low-energy region, that is, the contribution of exciton coupling does not seem relevant. We speculate that the major source of ECD signals is a twist of the conjugated backbone.[47] The freshly prepared **SC-1** sample was also characterized by microscopy techniques: both optical microscopy (Figure 6a) and FE-SEM analysis (Figure 6b) revealed a quite homogeneous texture.

A very different behaviour in thin films was observed in the case of TEG-functionalized chiral DPP-triazole dye **2**, showing a definitely higher variability in the solid-state aggregation. The ECD spectrum of drop-cast sample **DC-2** (Figure 5b) showed a positive exciton couplet between 450 nm and 700 nm with maximum intensity at 661 nm ($g_{abs} = +9.26\times10^{-3}$) and 549 nm ($g_{abs} = -6.84\times10^{-3}$), indicating the occurrence of a right-handed supramolecular helical stack. This couplet is associated to the main band of the corresponding UV–vis absorption spectrum of **DC-2** (Figure S34) attributable to a $\pi\rightarrow\pi^*$ transition; two further negative narrow bands with stronger intensity fell in the higher energy region, at 412 nm ($g_{abs} = -1.78\times10^{-2}$) and at 339 nm ($g_{abs} = -2.01\times10^{-2}$). In this case, if solvent annealing was responsible for only minor changes in the ECD spectrum (Figure S35), with a flattening of the positive exciton couplet in the low energy region, thermal annealing resulted in a complete disappearance of the ECD spectrum, despite maintaining the same UV–vis absorption profile (Figure S36). While the modest molecular mobility due to solvent annealing was responsible for minimal rearrangements of the right-handed supramolecular helix, the molecular mobility induced by high temperatures was strong enough to disrupt chiral aggregates. A further different situation was found in the case of spin-coated sample **SC-2**: the ECD spectrum (Figure 5c) showed a very different profile, though an asymmetric positive exciton couplet seems to be retained between 450 nm and 700 nm, with a quite intense positive band centred at 635 nm ($g_{abs} = +8.01\times10^{-3}$) and a smaller negative band having maximum at 498 nm ($g_{abs} = -2.55\times10^{-3}$).

This result suggests the organization of DPP-triazole dye molecules into a quite different aggregation mode, although presumably still consisting of right-handed helical architectures. It is worth emphasizing that the identification of two different aggregation modes for **DC-2** and **SC-2** was only made possible by ECD spectroscopy, since the UV–vis absorption spectra of **SC-2** (Figure S37) and **DC-2** were very similar: a broad band between 450 and 700 nm with maximum at 632 nm, attributable to a $\pi\rightarrow\pi^*$ transition, and two further bands at higher energy with maximum at 408 and 329 nm. Such difference in the aggregation modes of **DC-2** and **SC-2** samples was not even detected by microscopy: optical microscopy images of **DC-2** (Figure 6c) and **SC-2** (Figure 6e) revealed a quite similar and homogeneous texture, while in the FE-SEM images of both **DC-2** (Figure 6d) and **SC-2** (Figure 6f) we appreciated the

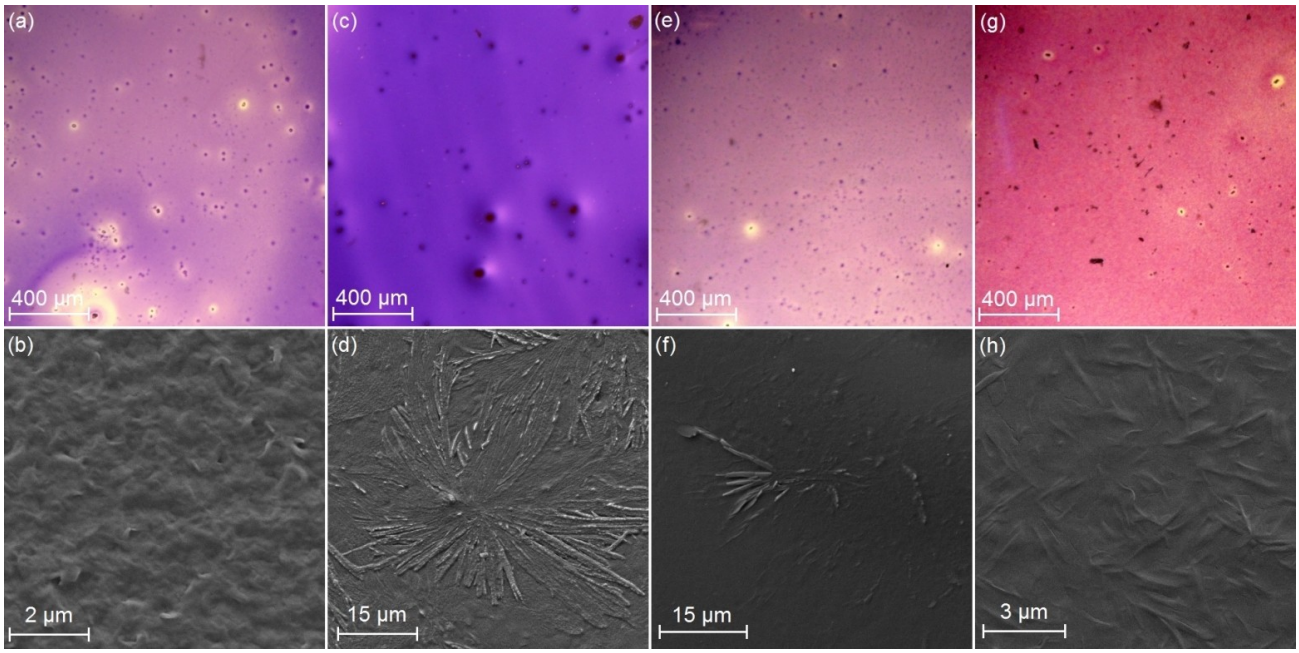

Figure 6. Microscopy characterization of chiral DPP-triazole dyes **1**–**3** in thin films obtained under the most relevant experimental conditions. Optical microscopy images of freshly prepared a) **SC-1**, c) **DC-2** and e) **SC-2**, as well as g) **SC-3** after solvent annealing. FE-SEM images of freshly prepared b) **SC-1**, d) **DC-2** and f) **SC-2**, as well as h) **SC-3** after solvent annealing.

formation of radially symmetrical crystallites (size of ca. 10–20 μm), each of them in turn consisting of thinner fibres with a diameter of about 10 nm. Moving on post-deposition operations, the spin-coated sample **SC-2** exhibited a behaviour quite similar to **DC-2**: solvent annealing did not lead to appreciable variations in the UV–vis and ECD spectra (Figure S38), while thermal annealing completely knocked down the dichroic signals (Figure S39) probably due to a weakening of the intermolecular interactions holding together the DPP-triazole molecules in the aforementioned fibres caused by the high temperature.

The *t*-Boc-functionalized chiral DPP-triazole dye **3** also showed considerable variety in the solid-state aggregation, although in a different way from compound **2**. A first very interesting aspect is that freshly prepared thin films of **3** did not show any ECD signal, both for drop-cast samples **DC-3** and spin-coated samples **SC-3** (Figures S40 and S43, respectively). This could be due to the presence of ordered structures with co-facial stacking of adjacent molecules, or alternatively to the presence of a disordered structure; less probable, although not to be excluded, could be the presence of a mixture of chiral supramolecular structures with opposite handedness whose ECD contributions would cancel each other. The poorly resolved vibronic structure of the corresponding UV–vis absorption spectra observed before solvent annealing (Figures S40 and S43) suggests the presence of a disordered supramolecular organization at this stage. Post-deposition operations produced drastic changes in the optical and chiroptical features of these samples. In particular, in the case of **SC-3** the application of solvent annealing resulted in the formation of strong dichroic signals in the ECD spectrum (Figure 5d), consisting of a strong, asymmetric positive exciton couplet between 400 and 700 nm, with the positive band having maximum intensity at 624 nm ($g_{abs} = +2.34 \times 10^{-2}$) and the negative band centred at 511 nm ($g_{abs} = -1.62 \times 10^{-2}$). Admittedly, the increased mobility acquired by the π-conjugated chains during solvent curing allowed for a significant supramolecular rearrangement into a right-handed supramolecular helix, responsible for strong chiroptical signals. The structural reorganization of **SC-3** into more ordered architectures after solvent annealing was also confirmed by UV–vis spectroscopy (Figure S44), where a more resolved vibronic structure of the absorption bands was found. The optical microscopy characterization of solvent-annealed **SC-3** sample showed a quite homogeneous texture (Figure 6g), although FE-SEM images revealed the presence of needle-like fibres, sized a few microns in length and a few nanometres in diameter (Figure 6h). Very surprisingly, the use of thermal annealing on sample **SC-3** allowed us to obtain an ECD spectrum of opposite sign with respect to the previous one, although with signals of very modest intensity (Figure S45), thus indicating the occurrence of a left-handed supramolecular organization of *t*-Boc-functionalized DPP-triazole molecules. The increased molecular mobility provided by high temperatures with respect to solvent annealing may allow the π-conjugated molecules to organize into a different stable aggregation mode, with opposite helicity. A similar behaviour was also found in the case of drop-cast sample **DC-3**: the ECD spectra of the sample after solvent annealing (Figure S41) and thermal annealing (Figure S42) were very different from each other and described two different supramolecular architectures, possibly endowed with opposite helicities (right-handed after solvent annealing and left-handed after thermal annealing).

For all thin film samples, we plotted dissymmetry factor g_{abs} values vs. wavelengths (Figures S28–S45), thus offering a more intuitive comparison about the strength of CP absorption for the three chiral DPP-triazole dyes **1**–**3**. In order to be sure that all calculated g_{abs} values were free of spurious contributions due to reflection (which is often a relevant source of artifacts in thin films), for most of thin film samples reflectance spectra were also measured (Figure S49): as expected, in all cases reflectance was found to be around 10%, which is about the same for the blank glass plates, thus confirming an almost negligible reflection contribution of the organic π-conjugated layers.

The data of both optical and chiroptical features of chiral DPP-triazole dyes **1**–**3** in thin films prepared under the most relevant experimental conditions (freshly prepared **SC-1**, freshly prepared **DC-2**, freshly prepared **SC-2**, solvent annealed **SC-3**) are summarized in Table S2. Furthermore, to fully confirm our results at least for the situations leading to the strongest chiroptical signals, we repeated some representative ECD measurements on the opposite enantiomer of dyes **1** and **2**, that is, compounds *ent*-**1** and *ent*-**2**: freshly prepared spin-coated sample **SC**-*ent*-**1** (Figure S46), drop-cast sample **DC**-*ent*-**2** (Figure S47) and spin-coated sample **SC**-*ent*-**2** (Figure S48). In all cases, we obtained perfectly mirror image ECD profiles to the opposite enantiomers, confirming the total reproducibility of our results.

The optical and chiroptical characterization of chiral DPP-triazole dyes **1**–**3** in thin films confirmed the relevant impact of *n*-octyl, TEG and *t*-Boc side groups on tuning their physico-chemical features: despite chiral DPP-triazole dyes **1**–**3** are functionalized with the same enantiopure (*S*)-(+)-citronellyl chains, the three different achiral groups on the lactam moieties are responsible for three different behaviours in the chiral supramolecular organization of these π-conjugated compounds in the solid state. In our opinion, this is a very important point: since the number of enantiopure alkyl chains from natural sources used as chiral substituents for π-conjugated systems is still quite limited (in most cases, β-citronellyl, 2-ethylhexyl and menthyl groups),[7b] the possibility of modulating the chiroptical properties in thin films by keeping the same enantiopure appendage is a crucial aspect for mastering and optimizing their possible performances in innovative technological devices.

Further insights into the impact of achiral *n*-octyl, TEG and *t*-Boc side groups on the solid state organization of chiral DPP-triazole dyes **1**–**3** can be obtained by means of powder X-ray diffraction (PXRD) measurements (Figure S50). Interestingly, we found that crystallinity decreased moving from *t*-Boc-functionalized dye **3**, whose diffraction pattern showed good crystallinity, to TEG-functionalized DPP-triazole **2** and, above all, *n*-octyl-functionalized DPP dye **1**, where an amorphous component clearly appeared. From these results it is clear that not only polarity, but also steric hindrance of side groups plays a crucial role in the solid state arrangements: on the one hand, despite its high steric hindrance exerted near the nitrogen atoms of the lactam rings, the more rigid and compact structure of *t*-Boc group allowed for a more effective packing of compound **3**, thus favouring a higher crystallinity; on the other hand, longer and more flexible TEG and *n*-octyl chains resulted in a less effective packing of, respectively, dyes **2** and **1** in the solid state, characterized by a lower crystallinity.

Putting together the structural evidence emerging from chiroptical data and PXRD measurements, we can infer the supramolecular organization of dyes **1**–**3** in the solid state as shown in Figure 7. The molecular modelling procedure used to generate the models is described in the Supporting Information. Molecules of dye **1** pack together loosely due to the flexibility of the alkyl chains; while no efficient intermolecular exciton coupling is possible, a twist of the conjugated moiety is allowed which generates a monosignated ECD spectrum. The molecules of dye **2** pack more strongly with a face-to-face arrangement of the conjugated moieties yielding a moderately strong exciton-coupled ECD. The TEG chains, though assuming their preferred *gauche* conformation, impart some disorder to the aggregate, which remains semi-crystalline. Finally, dye **3** packs quite tightly thanks to the compactness of the *t*-Boc group. The regular arrangement favours strong exciton-coupled ECD spectra with vibronic structure and a high degree of crystallinity.

Finally, the thermal properties of chiral DPP-triazole dyes **1**–**3** were investigated by differential scanning calorimetry (DSC) analysis. As expected, the different length and polarity of the groups on the nitrogen atoms of DPP moieties were responsible for very dissimilar DSC profiles, as depicted in Figure 8. In the

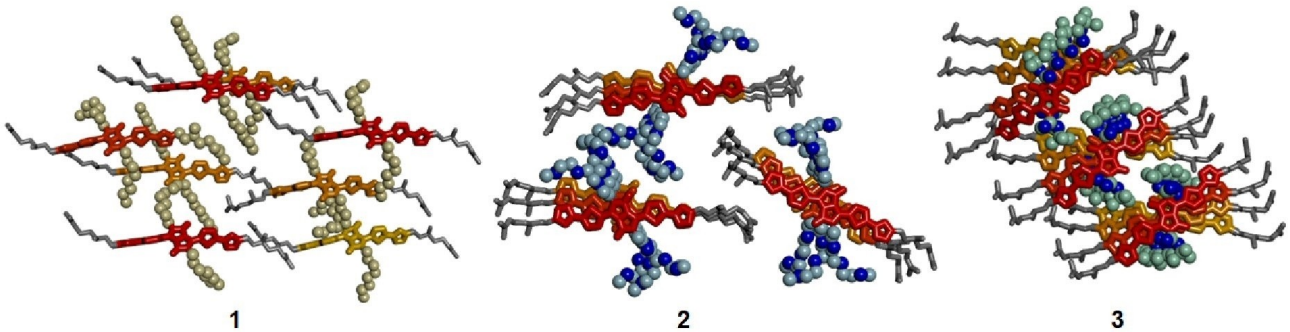

Figure 7. Pictorial representation of the aggregation modes of dyes **1**–**3**. The conjugated moiety is represented by broad sticks in red-orange hues, the chiral chain by thin grey sticks, and the R groups by spheres in light hues (oxygen atoms in blue).

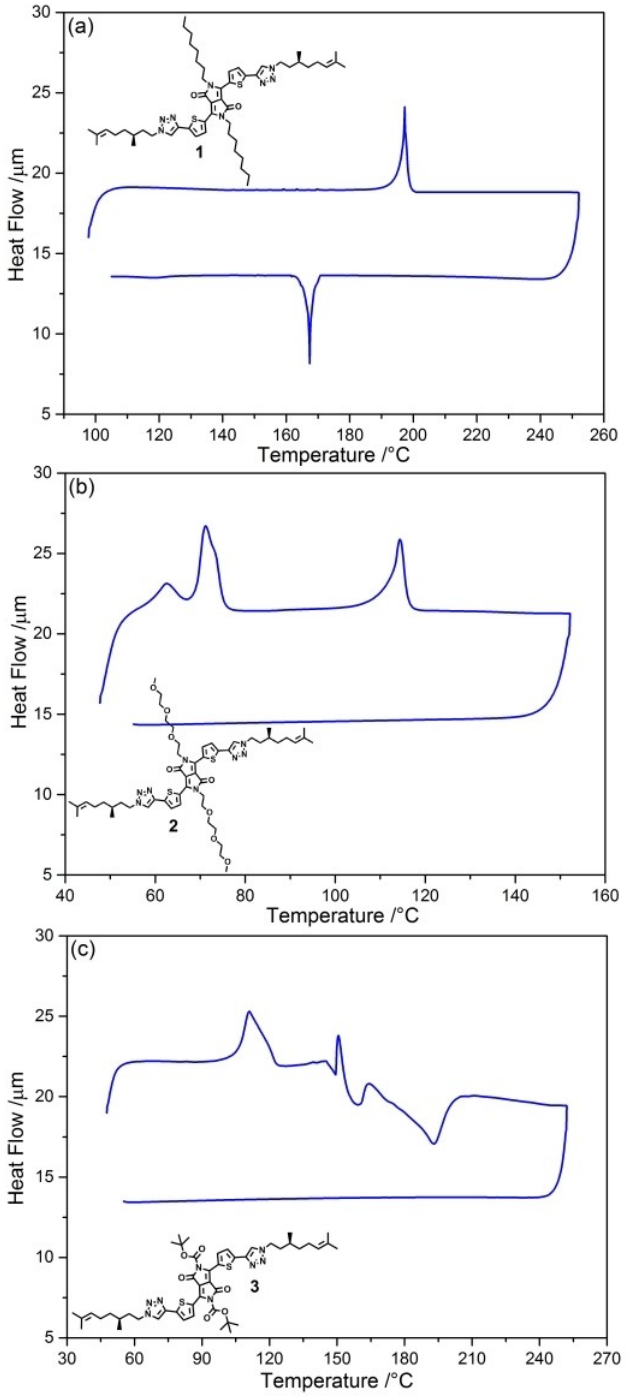

Figure 8. Differential scanning calorimetry (DSC) thermograms of a) *n*-octyl-functionalized DPP-triazole dye **1**, b) TEG-functionalized DPP-triazole dye **2** and c) *t*-Boc-functionalized DPP-triazole dye **3** recorded at a scan rate of 10 °C min^{-1}.

case of *n*-octyl-functionalized dye **1**, we observed only one phase transition (Figure 8a): an exothermic transition (solid phase→liquid phase) at around 198 °C on heating, and an endothermic transition (liquid phase→solid phase) at 167–168 °C on cooling. The TEG-decorated dye **2** showed a more complex DSC profile (Figure 8b), with three exothermic peaks (at 65, 72 and 115 °C) on heating and no transition in the subsequent cooling; this suggested the possibility of thermal decomposition.

In the case of compound **3**, bearing the thermo-cleavable *t*-Boc group, the occurrence of a thermal degradation was not surprising: a very complex DSC profile was observed on heating, with both exothermic and endothermic transitions (Figure 8c), indicating the existence of several phases before the thermo-cleavage of *t*-Boc groups to the corresponding N–H-free DPP-triazole dye (characterized by a significantly higher melting temperature, due to the formation of strong C=O···H–N hydrogen bonds).[37c]

Conclusion

In conclusion, in this work we have reported the synthesis and characterization of three new chiral DPP-triazole dyes bearing enantiopure β-citronellyl units on the terminal positions of a π-conjugated backbone, and differing in the presence of very diverse groups on the nitrogen atoms of the lactam moieties. The hydrophobic and apolar *n*-octyl chain of dye **1** is likely to assume an extended conformation and to be prone to interdigitation between neighbouring molecules. The hydrophilic and moderately polar TEG chain of dye **2** has a propensity for the nonplanar *gauche* conformation. The very bulky, thermocleavable and strongly polar *t*-Boc group was used in dye **3**. Besides electronic features, these three groups also differ significantly in their steric properties: on the one hand, the *t*-Boc group, despite its high steric hindrance exerted near the nitrogen atoms of the lactam rings, here ensured an effective packing of adjacent molecules into supramolecular aggregates thanks to its rigid and compact structure; on the other hand, the long and more flexible *n*-octyl and TEG chains, typically characterized by an overall lower grade of steric hindrance in the proximity of the nitrogen atoms of DPP moieties, were here responsible for a less effective packing between adjacent molecules. Despite keeping the same π-conjugated backbone and chiral units, we observed the occurrence of significantly different optical, chiroptical, electrochemical and thermal features in solution, solution aggregates and thin films: in this way, we revealed the central role played by achiral side chains in the aggregation modes of chiral organic materials at different hierarchical levels. In other words, by modulating the conformational, electronic and steric features of the side groups, it is possible to obtain widely different physicochemical properties for the same π-conjugated structure and chiral moiety.

To a very large extent, the achiral side groups determine the chiroptical properties of our DPP-triazole dyes **1**–**3** in solution aggregates and thin films. This is an important lesson: supramolecular chirality is the result of a combination of various contributions and it is far from being determined only by local stereogenic elements. As the typical enantiopure alkyl chains from natural sources used for this purpose are quite limited, the possibility of modulating the chiroptical properties of π-conjugated systems by keeping the same chiral appendage is a very important point. ECD reveals the occurrence of diverse

aggregation modes in samples that would look identical when using optical spectroscopy and microscopy techniques. In some cases, very strong chiroptical signals were found in thin films, with dissymmetry factor g_{abs} values up to 0.03. Both the intensity and tunability of the chiroptical signals of these organic materials might have major implications in the context of chiral organic optoelectronics and in the development of other highly innovative technological applications.

Experimental Section

Synthesis

General remarks: 3,6-Bis(5-bromothiophen-2-yl)-2,5-dioctylpyrrolo[3,4-*c*]pyrrole-1,4(2*H*,5*H*)-dione (**4a**),[48] 3,6-bis(5-bromothiophen-2-yl)-2,5-bis(2-(2-(2-methoxyethoxy)ethoxy)ethyl)pyrrolo[3,4-*c*]pyrrole-1,4(2*H*,5*H*)-dione (**4b**),[37c] and *tert*-butyl 3,6-bis(5-bromothiophen-2-yl)-1,4-dioxopyrrolo[3,4-*c*]pyrrole-2,5(1*H*,4*H*)-dicarboxylate (**4c**)[37c] were synthesized according to literature procedures. (*S*)-citronellyl azide (*S*)-**8** and (*R*)-citronellyl azide (*R*)-**8** were synthesized according to literature procedure[42] starting from, respectively, (*S*)-(+)-citronellyl bromide and (*R*)-(−)-citronellyl bromide, both available from Sigma-Aldrich by chemical synthesis at >95% purity. Compounds *ent*-**1** and *ent*-**2** were synthesized according to procedures described in Supporting Information. All the other reagents were purchased at the highest commercial quality from Sigma–Aldrich and used without further purification. Solvents were purified by conventional methods, distilled and stored under N_2. Preparative column chromatography was carried out using Macherey–Nagel silica gel (60, particle size 0.063–0.2 mm). Macherey–Nagel aluminium sheets with silica gel 60 F254 were used for TLC analyses. New compounds were characterized by ^{1}H NMR, ^{13}C NMR and HR–MS analysis. ^{1}H NMR and ^{13}C NMR spectra were acquired on an Agilent 500 spectrometer at 500 and at 125 MHz, respectively, using the $CDCl_3$ residual proton peak at $\delta = 7.26$ ppm as internal standard for ^{1}H spectra and the signals of $CDCl_3$ at $\delta = 77.16$ ppm as internal standard for ^{13}C spectra. High-resolution mass spectra were acquired with a Shimadzu high-performance liquid chromatography ion trap time-of flight (LC–IT–TOF) mass spectrometer by direct infusion of the samples by using methanol as the elution solvent (the samples were previously dissolved in THF, and few drops of the THF solution were added to methanol). Melting points were determined on a Reichert Microscope or on a Stuart Scientific Melting point apparatus SMP3.

2,5-Dioctyl-3,6-bis(5-((trimethylsilyl)ethynyl)thiophen-2-yl)pyrrolo[3,4-*c*]pyrrole-1,4(2*H*,5*H*)-dione (6a): Compound **6a** was synthesized according to a modified literature procedure.[49] A three-necked, round bottom flask equipped with a magnetic stirrer and a condenser was charged under N_2 with 3,6-bis(5-bromothiophen-2-yl)-2,5-dioctylpyrrolo[3,4-*c*]pyrrole-1,4(2*H*,5*H*)-dione (**4a**) (300 mg, 0.44 mmol), $Pd(OAc)_2$ (5.1 mg, 0.023 mmol), PPh_3 (17.4 mg, 0.066 mmol), CuI (4.3 mg, 0.023 mmol), triethylamine (15 mL) and dry CH_2Cl_2 (45 mL). The resulting mixture was cooled at 0 °C and stirred for 30 min, then (trimethylsilyl)acetylene **5** (183 μL, 1.32 mmol) was added. After a further 30 min at 0 °C, the reaction mixture was stirred for 24 h at 65 °C; then, it was cooled to room temperature, quenched with a saturated aqueous solution of NH_4Cl (50 mL) and extracted with CH_2Cl_2 (3×100 mL). The combined organic layer was washed with brine (3×50 mL), dried with anhydrous Na_2SO_4 and concentrated under vacuum. The crude product was purified by column chromatography on silica gel (*n*-hexane/CH_2Cl_2/ethyl acetate 9:1:1), affording product **6a** as a dark purple solid (240 mg, 76% yield). Spectroscopic data agree with those previously reported in the literature.[49] ^{1}H NMR (500 MHz, $CDCl_3$): δ 8.86 (d, J=4.1 Hz, 2H), 7.33 (d, J=4.1 Hz, 2H), 4.03 (t, J=7.6 Hz, 4H), 1.76–1.68 (m, 4H), 1.45–1.39 (m, 4H), 1.38–1.24 (m, 16H), 0.87 (t, J=7.0 Hz, 6H), 0.28 ppm (s, 18H). ^{13}C NMR (125 MHz, $CDCl_3$): δ 161.2, 139.2, 135.4, 133.9, 130.5, 128.5, 108.8, 104.4, 96.8, 42.4, 31.9, 30.1, 29.3, 29.3, 27.0, 22.7, 14.2, −0.2 ppm.

2,5-Bis(2-(2-(2-methoxyethoxy)ethoxy)ethyl)-3,6-bis(5-((trimethylsilyl)ethynyl)thiophen-2-yl)pyrrolo[3,4-*c*]pyrrole-1,4(2*H*,5*H*)-dione (6b): Compound **6b** was synthesized according to a modified literature procedure.[37c] A three-necked, round bottom flask equipped with a magnetic stirrer and a condenser was charged under N_2 with 3,6-bis(5-bromothiophen-2-yl)-2,5-bis(2-(2-(2-methoxyethoxy)ethoxy)ethyl)pyrrolo[3,4-*c*] pyrrole-1,4(2*H*,5*H*)-dione (**4b**) (300 mg, 0.40 mmol), $Pd(PPh_3)_4$ (23.1 mg, 0.02 mmol), CuI (7.6 mg, 0.04 mmol) and triethylamine (10 mL), then (trimethylsilyl)acetylene **5** (222 μL, 1.60 mmol) was added. The resulting mixture was stirred for 4 h at 60 °C; then, it was cooled to room temperature, quenched with a saturated aqueous solution of NH_4Cl (30 mL) and extracted with CH_2Cl_2 (3×50 mL). The combined organic layer was washed with brine (3×50 mL), dried with anhydrous Na_2SO_4 and concentrated under vacuum. The crude product was purified by column chromatography on silica gel (CH_2Cl_2/ethyl acetate = 8:2), affording product **6b** as a dark purple solid (198 mg, 63% yield). Spectroscopic data agree with those previously reported in the literature.[37c] ^{1}H NMR (500 MHz, $CDCl_3$): δ 8.65 (d, J=4.0 Hz, 2H), 7.26 (d, J=4.0 Hz, 2H), 4.19 (t, J=6.0 Hz, 4H), 3.73 (t, J=6.0 Hz, 4H), 3.60-3.58 (m, 4H), 3.54–3.51 (m, 8H), 3.45–3.42 (m, 4H), 3.30 (s, 6H), 0.22 ppm (s, 18H). ^{13}C NMR (125 MHz, $CDCl_3$): δ 161.4, 139.6, 134.9, 133.5, 130.4, 128.7, 108.9, 104.4, 96.8, 72.0, 70.9, 70.7, 70.6, 69.0, 59.1, 42.2, −0.2 ppm.

Di-*tert*-butyl 1,4-dioxo-3,6-bis(5-((trimethylsilyl)ethynyl)thiophen-2-yl)pyrrolo[3,4-*c*]pyrrole-2,5(1*H*,4*H*)-dicarboxylate (6c): Compound **6c** was synthesized according to a modified literature procedure.[37c] A three-necked, round bottom flask equipped with a magnetic stirrer and a condenser was charged under N_2 with di-*tert*-butyl 3,6-bis(5-bromothiophen-2-yl)-1,4-dioxopyrrolo[3,4-*c*]pyrrole-2,5(1*H*,4*H*)-dicarboxylate (**4c**) (300 mg, 0.456 mmol), $Pd(PPh_3)_2Cl_2$ (16 mg, 0.023 mmol), CuI (8.7 mg, 0.046 mmol), triethylamine (100 μL) and dry THF (30 mL), then (trimethylsilyl)acetylene **5** (194 μL, 1.82 mmol) was added. The resulting mixture was stirred for 4 h at 60 °C; then, it was cooled to room temperature, quenched with a saturated aqueous solution of NH_4Cl (50 mL) and extracted with CH_2Cl_2 (3×100 mL). The combined organic layer was washed with brine (3×50 mL), dried with anhydrous Na_2SO_4 and concentrated under vacuum. The crude product was purified by column chromatography on silica gel (*n*-hexane/CH_2Cl_2 = 2:8), affording product **6c** as a dark purple solid (190 mg, 60% yield). Spectroscopic data agree with those previously reported in the literature.[37c] ^{1}H NMR (500 MHz, $CDCl_3$): δ 8.11 (d, J=4.0 Hz, 2H), 7.21 (d, J=4.0 Hz, 2H), 1.59 (s, 18 H), 0.24 ppm (s, 18 H). ^{13}C NMR (125 MHz, $CDCl_3$): δ 158.9, 148.9, 136.9, 134.0, 133.2, 130.3, 130.0, 111.1, 104.9, 96.8, 86.3, 27.9, −0.2 ppm.

3,6-Bis(5-ethynylthiophen-2-yl)-2,5-dioctylpyrrolo[3,4-*c*]pyrrole-1,4(2*H*,5*H*)-dione (7a): Compound **7a** was synthesized according to a modified literature procedure.[49] 2,5-Dioctyl-3,6-bis(5-((trimethylsilyl)ethynyl)thiophen-2-yl)pyrrolo[3,4-*c*]pyrrole-1,4(2*H*,5*H*)-dione (**6a**) (240 mg, 0.335 mmol) and KF (195 mg, 3.35 mmol) were dissolved in THF (14 mL) and H_2O (6 mL). The resulting mixture was stirred at room temperature for 6 h, then it was quenched with a saturated aqueous solution of NH_4Cl (20 mL) and extracted with CH_2Cl_2 (3×50 mL). The combined organic layer was washed with brine (3×30 mL), dried with anhydrous Na_2SO_4 and concentrated under vacuum, affording product **7a** as a dark purple solid (188 mg, 98% yield). Spectroscopic data agree with those previ-

ously reported in the literature.[49] ^{1}H NMR (500 MHz, $CDCl_3$): δ 8.86 (d, J=4.1 Hz, 2H), 7.39 (d, J=4.1 Hz, 2H), 4.03 (t, J=7.5 Hz, 4H), 3.60 (s, 2H), 1.76–1.68 (m, 4H), 1.45–1.38 (m, 4H), 1.37–1.22 (m, 16H), 0.87 ppm (t, J=6.6 Hz, 6H). ^{13}C NMR (125 MHz, $CDCl_3$): δ 161.2, 139.4, 135.3, 134.3, 130.8, 127.3, 108.9, 85.7, 76.4, 42.5, 31.9, 30.2, 29.3 (2 C), 27.0, 22.8, 14.2 ppm.

3,6-Bis(5-ethynylthiophen-2-yl)-2,5-bis(2-(2-(2-methoxyethoxy)ethoxy)ethyl)pyrrolo[3,4-*c*]pyrrole-1,4(2*H*,5*H*)-dione (7 b): Compound **7 b** was synthesized according to a modified literature procedure.[37c] 2,5-Bis(2-(2-(2-methoxyethoxy)ethoxy)ethyl)-3,6-bis(5-((trimethylsilyl)ethynyl)thiophen-2-yl)pyrrolo[3,4-*c*]pyrrole-1,4(2*H*,5*H*)-dione (**6 b**) (307 mg, 0.39 mmol) and KF (227 mg, 3.91 mmol) were dissolved in THF (15 mL) and H_2O (5 mL). The resulting mixture was stirred at room temperature for 6 h, then it was quenched with a saturated aqueous solution of NH_4Cl (20 mL) and extracted with CH_2Cl_2 (3×50 mL). The combined organic layer was washed with brine (3×30 mL), dried with anhydrous Na_2SO_4 and concentrated under vacuum, affording product **7 b** as a dark purple solid (248 mg, 99% yield). Spectroscopic data agree with those previously reported in the literature.[37c] ^{1}H NMR (500 MHz, $CDCl_3$): δ 8.65 (d, J=4.0 Hz, 2H), 7.32 (d, J=4.0 Hz, 2H), 4.20 (t, J=6.0 Hz, 4H), 3.74 (t, J=6.0 Hz, 4H), 3.61–3.58 (m, 4H), 3.56–3.52 (m, 10H), 3.46–3.44 (m, 4H), 3.31 ppm (s, 6H). ^{13}C NMR (125 MHz, $CDCl_3$): δ 161.4, 139.8, 134.8, 134.0, 130.8, 127.4, 109.0, 85.6, 76.4, 72.0, 70.9, 70.7, 70.6, 69.0, 59.1, 42.3 ppm.

Di-*tert*-butyl 3,6-bis(5-ethynylthiophen-2-yl)-1,4-dioxopyrrolo[3,4-*c*]pyrrole-2,5(1*H*,4*H*)-dicarboxylate (7 c): Compound **7 c** was synthesized according to a modified literature procedure.[37c] Di-*tert*-butyl 1,4-dioxo-3,6-bis(5-((trimethylsilyl)ethynyl)thiophen-2-yl)pyrrolo[3,4-*c*]pyrrole-2,5(1*H*,4*H*)-dicarboxylate (**6 c**) (228 mg, 0.329 mmol) and KF (191 mg, 3.29 mmol) were dissolved in THF (20 mL) and H_2O (5 mL). The resulting mixture was stirred at room temperature for 6 h, then it was quenched with a saturated aqueous solution of NH_4Cl (30 mL) and extracted with CH_2Cl_2 (3×60 mL). The combined organic layer was washed with brine (3×50 mL), dried with anhydrous Na_2SO_4 and concentrated under vacuum, affording product **7 c** as a dark purple solid (190 mg, 90% yield). Spectroscopic data agree with those previously reported in the literature.[37c] ^{1}H NMR (500 MHz, $CDCl_3$): δ 8.16 (d, J=4.0 Hz, 2H), 7.28 (d, J=4.0 Hz, 2H), 3.56 (s, 2H), 1.59 ppm (s, 18H). ^{13}C NMR (125 MHz, $CDCl_3$), δ 158.9, 148.8, 137.1, 134.0, 133.7, 130.7, 128.6, 111.3, 86.5, 86.0, 76.4, 27.9 ppm.

3,6-Bis(5-(1-((*S*)-3,7-dimethyloct-6-en-1-yl)-1*H*-1,2,3-triazol-4-yl)thiophen-2-yl)-2,5-dioctylpyrrolo[3,4-*c*]pyrrole-1,4(2*H*,5*H*)-dione (1): A round bottom flask equipped with a magnetic stirrer and a condenser was charged with 3,6-bis(5-ethynylthiophen-2-yl)-2,5-dioctylpyrrolo[3,4-*c*]pyrrole-1,4(2*H*,5*H*)-dione (**7 a**) (188 mg, 0.328 mmol), (*S*)-citronellyl azide (*S*)-**8** (178 mg, 0.982 mmol), $Cu(OAc)_2\cdot H_2O$ (13.2 mg, 0.066 mmol) and H_2O (20 mL). The resulting mixture was stirred for 24 h at 80 °C; then, it was cooled to room temperature, quenched with a saturated aqueous solution of NH_4Cl (30 mL) and extracted with CH_2Cl_2 (3×60 mL). The combined organic layer was washed with brine (3×50 mL), dried with anhydrous Na_2SO_4 and concentrated under vacuum. The crude product was purified by column chromatography on silica gel (CH_2Cl_2/ethyl acetate = 95:5→4:1), affording product **1** as a dark purple solid (206 mg, 67% yield). M.p. 191–194 °C. ^{1}H NMR (500 MHz, $CDCl_3$): δ 8.98 (br s, 2H), 7.80 (s, 2H), 7.44 (d, J=4.1 Hz, 2H), 5.05 (t like, J=7.1 Hz, 2H), 4.47–4.36 (m, 4H), 4.09 (t, J=7.5 Hz, 4H), 2.06–1.90 (m, 6H), 1.81–1.71 (m, 6H), 1.66 (s, 6H), 1.58 (s, 6H), 1.54–1.19 (m, 26H), 0.98 (d, J=6.6 Hz, 6H), 0.84 ppm (t, J=6.9 Hz, 6H). ^{13}C NMR (125 MHz, $CDCl_3$): δ 161.3, 141.9, 139.6, 138.5, 136.4, 131.9, 129.1, 125.3, 124.2, 120.0, 108.2, 49.0, 42.4, 37.4, 36.8, 31.9, 30.2, 30.0, 29.4, 29.3, 27.0, 25.8, 25.4, 22.7, 19.3, 17.8, 14.2 ppm (one coincident signal not observed). HR–MS (LC–IT–TOF) m/z calcd. for $C_{54}H_{78}N_8O_2S_2$: 957.5581 $[M+Na]^+$; found: 957.5583.

3,6-Bis(5-(1-((*S*)-3,7-dimethyloct-6-en-1-yl)-1*H*-1,2,3-triazol-4-yl)thiophen-2-yl)-2,5-bis(2-(2-(2-methoxyethoxy)ethoxy)ethyl)pyrrolo[3,4-*c*]pyrrole-1,4(2*H*,5*H*)-dione (2): A round bottom flask equipped with a magnetic stirrer and a condenser was charged with 3,6-bis(5-ethynylthiophen-2-yl)-2,5-bis(2-(2-(2-methoxyethoxy)ethoxy)ethyl)pyrrolo[3,4-*c*]pyrrole-1,4(2*H*,5*H*)-dione (**7 b**) (200 mg, 0.312 mmol), (*S*)-citronellyl azide (*S*)-**8** (227 mg, 1.25 mmol), $Cu(OAc)_2\cdot H_2O$ (12.4 mg, 0.062 mmol) and H_2O (25 mL). The resulting mixture was stirred for 24 h at 80 °C; then, it was cooled to room temperature, quenched with a saturated aqueous solution of NH_4Cl (30 mL) and extracted with CH_2Cl_2 (3×60 mL). The combined organic layer was washed with brine (3×50 mL), dried with anhydrous Na_2SO_4 and concentrated under vacuum. The crude product was purified by column chromatography on silica gel (CH_2Cl_2/acetone 9:1→85:15→8:2), affording product **2** as a dark purple solid (188 mg, 60% yield). M.p. 113–115 °C. ^{1}H NMR (500 MHz, $CDCl_3$): δ 8.84 (br s, 2H), 7.86 (br s, 2H), 7.49 (br s, 2H), 5.05 (t, J=6.9 Hz, 2H), 4.48–4.36 (m, 4H), 4.35–4.26 (m, 4H), 3.80 (t, J=5.1 Hz, 4H), 3.66–3.62 (m, 4H), 3.61–3.53 (m, 8H), 3.46–3.43 (m, 4H), 3.30 (s, 6H), 2.05–1.91 (m, 6H), 1.81–1.72 (m, 2H), 1.66 (s, 6H), 1.58 (s, 6H), 1.54–1.45 (m, 2H), 1.43–1.35 (m, 2H), 1.28–1.20 (m, 2H), 0.98 ppm (d, J=6.3 Hz, 6H). ^{13}C NMR (125 MHz, $CDCl_3$): δ 161.5, 141.6, 139.9, 138.7, 136.1, 131.9, 128.8, 125.1, 124.2, 120.2, 108.3, 72.0, 70.9, 70.6, 69.1, 59.1, 49.0, 42.1, 37.4, 36.8, 30.0, 25.8, 25.4, 19.3, 17.8 ppm (two coincident signals not observed). HR–MS (LC–IT–TOF) m/z calcd. for $C_{52}H_{74}N_8O_8S_2$: 1025.4963 $[M+Na]^+$; found: 1025.4944.

Di-*tert*-butyl 3,6-bis(5-(1-((*S*)-3,7-dimethyloct-6-en-1-yl)-1*H*-1,2,3-triazol-4-yl)thiophen-2-yl)-1,4-dioxopyrrolo[3,4-*c*]pyrrole-2,5(1*H*,4*H*)-dicarboxylate (3): A round bottom flask equipped with a magnetic stirrer and a condenser was charged with di-*tert*-butyl 3,6-bis(5-ethynylthiophen-2-yl)-1,4-dioxopyrrolo[3,4-*c*]pyrrole-2,5(1*H*,4*H*)-dicarboxylate (**7 c**) (190 mg, 0.297 mmol), (*S*)-citronellyl azide (*S*)-**8** (323 mg, 1.78 mmol), sodium ascorbate (35.3 mg, 0.178 mmol), $Cu(OAc)_2\cdot H_2O$ (20.8 mg, 0.104 mmol), THF (15 mL) and H_2O (15 mL). The resulting mixture was stirred for 4 h at 65 °C; then, it was cooled to room temperature, quenched with a saturated aqueous solution of NH_4Cl (50 mL) and extracted with CH_2Cl_2 (3×100 mL). The combined organic layer was washed with brine (3×50 mL), dried with anhydrous Na_2SO_4 and concentrated under vacuum. The crude product was purified by column chromatography on silica gel (*n*-hexane/CH_2Cl_2/ethyl acetate 3:2:2), affording product **3** as a dark purple solid (114 mg, 42% yield). Darkening of the product was observed upon heating. ^{1}H NMR (500 MHz, $CDCl_3$): δ 8.30 (d, J=4.0 Hz, 2H), 7.78 (s, 2H), 7.46 (d, J=4.0 Hz, 2H), 5.06 (t, J=7.1 Hz, 2H), 4.48–4.37 (m, 4H), 2.06–1.92 (m, 6H), 1.81–1.71 (m, 2H), 1.67 (s, 6H), 1.63 (s, 18H), 1.59 (s, 6H), 1.56–1.47 (m, 2H), 1.44–1.36 (m, 2H), 1.31–1.21 (m, 2H), 0.99 ppm (d, J=6.6 Hz, 6H). ^{13}C NMR (125 MHz, $CDCl_3$): δ 159.2, 149.0, 141.8, 139.8, 137.4, 135.2, 131.9, 128.9, 125.0, 124.2, 120.2, 110.6, 86.2, 49.0, 37.4, 36.8, 30.0, 27.9, 25.9, 25.4, 19.3, 17.8 ppm (one coincident signal not observed). HR–MS (LC–IT–TOF) m/z calcd. for $C_{48}H_{62}N_8O_6S_2$: 933.4126; $[M+Na]^+$ found: 933.4119.

Characterization

Solution: UV–vis absorption measurements in solution were performed at room temperature with a Shimadzu UV-2401PC spectrophotometer, with temperature control to within ±0.1 °C. Photoluminescence emission measurements in solution were performed at room temperature using a Varian Cary Eclipse fluorescence spectrophotometer, with temperature control to within ±0.1 °C, at λ_{ex}=550 nm (for DPP-triazole dyes **1** and **2**) or

530 nm (for DPP-triazole dye **3**). Stock solutions of each dye in the solvent ($CHCl_3$, THF, toluene) were 10^{-2} M, while working solutions were 10^{-4} M for UV–vis absorption and 10^{-6} M for photoluminescence measurements.

Molar extinction coefficients ε were calculated in each solvent at two wavelengths of maximum absorbance, by using five working solutions of the DPP-triazole dye at different concentrations, from 2.0×10^{-7} to 1.0×10^{-6} M (Figures S3–S11 in Supporting Information). Fluorescence quantum yields ϕ, determined by the relative method using rhodamine B in absolute ethanol as the reference, were calculated in each solvent by using five working solutions of the DPP-triazole dye at different concentrations, from 2.0×10^{-7} to 1.0×10^{-6} M (Figures S12–S20). UV–vis absorption onset wavelengths λ_{onset} were determined from the intercept of the red-side slope of the absorbance main band with the wavelength axis (Figures S21–S23).

Cyclic voltammetry measurements were carried out with a Metrohm Autolab potentiostat (model PGSTAT128N) using a conventional three-electrode configuration consisting of a glassy carbon working electrode and platinum wires as the counter and reference electrodes. All cyclic voltammetry measurements were recorded at room temperature under nitrogen in anhydrous dichloromethane solution (scan rate 0.1 Vs^{-1}). The sample solutions were prepared as follows: a 0.1 M solution of nBu$_4$NPF$_6$ as the supporting electrolyte in anhydrous dichloromethane was prepared in a glovebox; the proper amount of compounds **1**–**3** was then dissolved in the desired volume of nBu$_4$NPF$_6$ solution at a final sample concentration of 9×10^{-4} M. All measurements were calibrated by using the Fc/Fc^+ redox couple as an external standard. The HOMO and LUMO energy levels were estimated by the empirical equations $HOMO=-e(E_{ox}+5.1\ V)$ and $LUMO=-e(E_{red}+5.1\ V)$, where E_{ox} is the average value between the oxidation potential peak and the related reverse one measured for the DPP-triazole dye in solution vs. Fc/Fc^+ reference; E_{red} is the average value between the reduction potential peak and the related reverse one measured for the DPP-triazole dye in solution vs. Fc/Fc^+ reference; 5.1 eV is the position of the formal potential of the Fc/Fc^+ redox couple on the Fermi scale.[50]

Solution aggregation: UV–vis absorption measurements under solution aggregation were performed at room temperature with a Jasco V-650 spectrophotometer. Electronic circular dichroism (ECD) measurements under solution aggregation were performed at room temperature with a Jasco J-710 spectropolarimeter. For each chiral DPP-triazole dye, solution aggregation was induced using solvent mixtures consisting of a good solvent and a poor solvent (i.e., $CHCl_3$/MeOH or THF/H_2O) in different ratio. Stock solutions of each dye in the good solvent (i.e., $CHCl_3$ or THF) were 10^{-2} M, while solution aggregation samples in $CHCl_3$/MeOH or THF/H_2O mixtures were 10^{-4} M. For each sample, the dissymmetry factor g_{abs} spectrum (Figures S26 and S27) was calculated as "ECD spectrum/UV–vis absorption spectrum", i.e., as $g_{abs}=(\text{ellipticity (mdeg)}\times32980)/\text{absorbance}$.

Thin films: Drop-cast (DC) samples were prepared by depositing dropwise on a glass plate ~100 μL of a 2.0×10^{-3} M solution of the chiral DPP-triazole dye in $CHCl_3$, followed by slow evaporation of the solvent in an atmosphere saturated with $CHCl_3$ vapours. Spin coated (SC) samples were prepared by spin coating ~100 μL of a 2.0×10^{-2} M solution of the chiral DPP-triazole dye in $CHCl_3$ on a glass plate, using a WS-650MZ-23NPPB (Laurell Technologies Corp., North Wales, PA, USA) spin-coater; conditions: 1000 rpm, 30 s, acceleration 1000 rpm/s. Solvent annealing was carried out by keeping thin film samples for 1 h in a closed chamber saturated with $CHCl_3$ vapours. Thermal annealing was carried out by keeping thin film samples for 1 h in an oven at 100 °C.

UV–vis absorption spectra in thin films were recorded at room temperature using a Jasco V-650 spectrophotometer. Electronic circular dichroism (ECD) spectra in thin films were recorded at room temperature using a Jasco J-710 spectropolarimeter. In all cases, at least 3 independent thin film samples were prepared and subjected to full absorbance and ECD analysis. For each thin film sample, the invariance of ECD spectrum upon rotation (i.e., at different rotational angles θ around the optical axis) and upon flipping (i.e., with the organic layer facing the light source, namely *front*, or the detector, namely *back*) was testified by four different measurements: front 0°, front 90°, back 0°, back 90° (Figures S28–S45). For each thin film sample, ECD spectra were normalized with respect to the maximum absorbance value of the same sample, in order to avoid any mistake possibly associated to inhomogeneity. For each thin film, the dissymmetry factor g_{abs} spectrum (Figures S28–S45) was calculated as "not normalized ECD spectrum/UV–vis absorption spectrum", that is, as $g_{abs}=(\text{not normalized ellipticity (mdeg)}/32980)/\text{absorbance}$. Reflectance measurements of thin films were recorded at room temperature over the wavelength range of 300–800 nm by using an Agilent Cary 5000 UV–vis-NIR spectrophotometer equipped with a 110 mm integration sphere (model: Internal DRA 2500 Agilent).

Optical microscopy images of thin films were obtained at room temperature using a Zeiss SteREO Discovery V8 microscope equipped with a Canon PowerShot A640 camera. Field-emission scanning electron microscopy (FE-SEM) images of thin films were acquired on a FEI Quanta 450 ESEM FEG instrument using secondary electron detection. The samples were coated with a 12 nm Pt layer.

Powder X-ray diffraction (PXRD) patterns were collected using a Bruker D2 Phaser diffractometer operating at 30 kV and 10 mA in $\theta-\theta$ scan mode with Ni-filtered $Cu_{K\alpha}$ radiation and equipped with a one-dimensional Lynxeye detector.

DSC measurements were carried out under nitrogen atmosphere with a Mettler Toledo STARe system DSC. The scan rate was 10 °C min^{-1}. For each chiral DPP-triazole sample, ~2–3 mg of solid compound were placed in standard Mettler aluminium crucibles. To avoid any influence of thermal decomposition on the thermal data, the first heating and cooling scan loop was only displayed.

Acknowledgements

This work was financially supported by MIUR, Ministero dell'Istruzione, dell'Università e della Ricerca (PRIN 2017 project "CHIRALAB", Prot. 20172M3K5N) and by Università di Pisa (PRA 2020_21). A. T. thanks the European Commission Research Executive Agency, Horizon 2020 Research, and Innovation Programme under the Marie Sklodowska-Curie grant agreement no. 859752-HEL4CHIROLED-H2020-MSCAITN-2019 for financial support. The authors thank the Centre for Instrumentation Sharing of the University of Pisa (CISUP, Dr. Randa Anis Ishak) for FE-SEM investigation of thin film samples. The authors also acknowledge the help of Alessia Iennaco in the synthesis of chiral DPP-triazole dye **3**, Eugenio Artusato in the preparation of thin-film samples of chiral DPP-triazole dye **2** for ECD investigation, Prof. Andrea Pucci and Cosimo Micheletti in the reflectance measurements of thin films, Dr. Daniela Mauro and Dr. Marzia Dell'Aera in the powder X-ray diffraction measurements and discussion, and Dr. Vito Rizzi in the DSC analysis of the three chiral DPP-triazole dyes. Open Access funding

provided by Università degli Studi di Pisa within the CRUI-CARE Agreement.

Conflict of Interest

The authors declare no conflict of interest.

Data Availability Statement

The data that support the findings of this study are available from the corresponding author upon reasonable request.

Keywords: chirality · diketopyrrolopyrroles · organic dyes · supramolecular chemistry · triazoles

[1] a) A. Facchetti, *Chem. Mater.* **2011**, *23*, 733–758; b) C. Wang, H. Dong, W. Hu, Y. Liu, D. Zhu, *Chem. Rev.* **2012**, *112*, 2208–2267; c) X. Guo, M. Baumgarten, K. Müllen, *Prog. Polym. Sci.* **2013**, *38*, 1832–1908; d) P. Friederich, A. Fediai, S. Kaiser, M. Konrad, N. Jung, W. Wenzel, *Adv. Mater.* **2019**, *31*, 1808256.
[2] J. Qi, Z. Chen, P. Jiang, W. Hu, Y. Wang, Z. Zhao, X. Cao, S. Zhang, R. Tao, Y. Li, D. Fang, *Adv. Sci.* **2022**, *9*, 2102662.
[3] a) J. Gierschner, J. Cornil, H.-J. Egelhaaf, *Adv. Mater.* **2007**, *19*, 173–191; b) O. Ostroverkhova, *Chem. Rev.* **2016**, *116*, 13279–13412.
[4] a) J. Cornil, D. Beljonne, J.-P. Calbert, J.-L. Brédas, *Adv. Mater.* **2001**, *13*, 1053–1067; b) F. J. M. Hoeben, P. Jonkheijm, E. W. Meijer, A. P. H. J. Schenning, *Chem. Rev.* **2005**, *105*, 1491–1546; c) T. L. Andrew, T. M. Swager, *J. Polym. Sci. Part B* **2011**, *49*, 476–498.
[5] a) A. Salleo, R. J. Kline, D. M. DeLongchamp, M. L. Chabinyc, *Adv. Mater.* **2010**, *22*, 3812–3838; b) J. Rivnay, S. C. B. Mannsfeld, C. E. Miller, A. Salleo, M. F. Toney, *Chem. Rev.* **2012**, *112*, 5488–5519.
[6] a) P. A. Korevaar, T. F. A. de Greef, E. W. Meijer, *Chem. Mater.* **2014**, *26*, 576–586; b) Y. Dorca, E. E. Greciano, J. S. Valera, R. Gómez, L. Sánchez, *Chem. Eur. J.* **2019**, *25*, 5848–5864.
[7] a) L. A. P. Kane-Maguire, G. G. Wallace, *Chem. Soc. Rev.* **2010**, *39*, 2545–2576; b) M. Verswyvel, G. Koeckelberghs, *Polym. Chem.* **2012**, *3*, 3203–3216; c) M. Liu, L. Zhang, T. Wang, *Chem. Rev.* **2015**, *115*, 7304–7397.
[8] a) C. Resta, S. Di Pietro, M. Majerić Elenkov, Z. Hameršak, G. Pescitelli, L. Di Bari, *Macromolecules* **2014**, *47*, 4847–4850; b) O. Hassan Omar, M. Falcone, A. Operamolla, G. Albano, *New J. Chem.* **2021**, *45*, 12016–12023.
[9] a) C. C. Lee, C. Grenier, E. W. Meijer, A. P. H. J. Schenning, *Chem. Soc. Rev.* **2009**, *38*, 671–683; b) Y. Yang, Y. Zhang, Z. Wei, *Adv. Mater.* **2013**, *25*, 6039–6049.
[10] C. Zhang, Y. Yan, Y. S. Zhao, J. Yao, *Acc. Chem. Res.* **2014**, *47*, 3448–3458.
[11] a) M. Hu, H.-T. Feng, Y.-X. Yuan, Y.-S. Zheng, B. Z. Tang, *Coord. Chem. Rev.* **2020**, *416*, 213329; b) A. Nitti, D. Pasini, *Adv. Mater.* **2020**, *32*, 1908021; c) C. Liu, J.-C. Yang, J. W. Y. Lam, H.-T. Feng, B. Z. Tang, *Chem. Sci.* **2022**, *13*, 611–632.
[12] a) Y. Yang, R. C. da Costa, M. J. Fuchter, A. J. Campbell, *Nat. Photonics* **2013**, *7*, 634–638; b) J. R. Brandt, F. Salerno, M. J. Fuchter, *Nat. Chem. Rev.* **2017**, *1*, 0045.
[13] a) G. Albano, L. A. Aronica, A. Minotto, F. Cacialli, L. Di Bari, *Chem. Eur. J.* **2020**, *26*, 16622–16627; b) D.-W. Zhang, M. Li, C.-F. Chen, *Chem. Soc. Rev.* **2020**, *49*, 1331–1343.
[14] J. G. Ibanez, M. E. Rincón, S. Gutierrez-Granados, M. H. Chahma, O. A. Jaramillo-Quintero, B. A. Frontana-Uribe, *Chem. Rev.* **2018**, *118*, 4731–4816.
[15] C. Wang, H. Fei, Y. Qiu, Y. Yang, Z. Wei, Y. Tian, Y. Chen, Y. Zhao, *Appl. Phys. Lett.* **1999**, *74*, 19–21.
[16] C. Train, M. Gruselle, M. Verdaguer, *Chem. Soc. Rev.* **2011**, *40*, 3297–3312.
[17] P. C. Mondal, C. Fontanesi, D. H. Waldeck, R. Naaman, *Acc. Chem. Res.* **2016**, *49*, 2560–2568.
[18] a) N. Berova, L. D. Bari, G. Pescitelli, *Chem. Soc. Rev.* **2007**, *36*, 914–931; b) G. Pescitelli, L. Di Bari, N. Berova, *Chem. Soc. Rev.* **2011**, *40*, 4603–4625; c) G. Pescitelli, L. Di Bari, N. Berova, *Chem. Soc. Rev.* **2014**, *43*, 5211–5233; d) G. Pescitelli, *Chirality* **2022**, *34*, 333–363.
[19] a) G. Albano, M. Lissia, G. Pescitelli, L. A. Aronica, L. Di Bari, *Mater. Chem. Front.* **2017**, *1*, 2047–2056; b) G. Albano, F. Salerno, L. Portus, W. Porzio, L. A. Aronica, L. Di Bari, *ChemNanoMat* **2018**, *4*, 1059–1070.
[20] a) F. S. Richardson, J. P. Riehl, *Chem. Rev.* **1977**, *77*, 773–792; b) J. P. Riehl, F. S. Richardson, *Chem. Rev.* **1986**, *86*, 1–16; c) G. Longhi, E. Castiglioni, J. Koshoubu, G. Mazzeo, S. Abbate, *Chirality* **2016**, *28*, 696–707; d) Y. He, S. Lin, J. Guo, Q. Li, *Aggregate* **2021**, *2*, e141; e) X.-M. Chen, S. Zhang, X. Chen, Q. Li, *ChemPhotoChem* **2022**, *6*, e202100256.
[21] a) P. Mayorga Burrezo, V. G. Jiménez, D. Blasi, I. Ratera, A. G. Campaña, J. Veciana, *Angew. Chem. Int. Ed.* **2019**, *58*, 16282–16288; *Angew. Chem.* **2019**, *131*, 16428–16434; b) P. Mayorga-Burrezo, V. G. Jiménez, D. Blasi, T. Parella, I. Ratera, A. G. Campaña, J. Veciana, *Chem. Eur. J.* **2020**, *26*, 3776–3781; c) F. Zinna, G. Albano, A. Taddeucci, T. Colli, L. A. Aronica, G. Pescitelli, L. Di Bari, *Adv. Mater.* **2020**, *32*, 2002575.
[22] G. Albano, F. Zinna, F. Urraci, M. A. M. Capozzi, G. Pescitelli, A. Punzi, L. Di Bari, G. M. Farinola, *Chem. Eur. J.* **2022**, *28*, e202201178.
[23] a) M. Grzybowski, D. T. Gryko, *Adv. Opt. Mater.* **2015**, *3*, 280–320; b) M. Kaur, D. H. Choi, *Chem. Soc. Rev.* **2015**, *44*, 58–77.
[24] a) Z. Hao, A. Iqbal, *Chem. Soc. Rev.* **1997**, *26*, 203–213; b) O. Wallquist, R. Lenz, *Macromol. Symp.* **2002**, *187*, 617–630.
[25] W. Li, L. Wang, H. Tang, D. Cao, *Dyes Pigm.* **2019**, *162*, 934–950.
[26] a) E. H. Ghazvini Zadeh, M. V. Bondar, I. A. Mikhailov, K. D. Belfield, *J. Phys. Chem. C* **2015**, *119*, 8864–8875; b) T. He, Y. Gao, S. Sreejith, X. Tian, L. Liu, Y. Wang, H. Joshi, S. Z. F. Phua, S. Yao, X. Lin, Y. Zhao, A. C. Grimsdale, H. Sun, *Adv. Opt. Mater.* **2016**, *4*, 746–755.
[27] C. B. Nielsen, M. Turbiez, I. McCulloch, *Adv. Mater.* **2013**, *25*, 1859–1880.
[28] a) T. Beyerlein, B. Tieke, S. Forero-Lenger, W. Brütting, *Synth. Met.* **2002**, *130*, 115–119; b) Z. Qiao, Y. Xu, S. Lin, J. Peng, D. Cao, *Synth. Met.* **2010**, *160*, 1544–1550; c) W. Kitisriworaphan, T. Chawanpunyawat, T. Manyum, P. Chasing, S. Namuangruk, T. Sudyoadsuk, V. Promarak, *RSC Adv.* **2021**, *11*, 12710–12719.
[29] W. Li, K. H. Hendriks, M. M. Wienk, R. A. J. Janssen, *Acc. Chem. Res.* **2016**, *49*, 78–85.
[30] K. Dhbaibi, L. Favereau, M. Srebro-Hooper, M. Jean, N. Vanthuyne, F. Zinna, B. Jamoussi, L. Di Bari, J. Autschbach, J. Crassous, *Chem. Sci.* **2018**, *9*, 735–742.
[31] T. Gao, Z. Jiang, B. Chen, Q. Sun, Y. Orooji, L. Huang, Z. Liu, *Dyes Pigm.* **2020**, *173*, 107998.
[32] P. A. Hume, J. P. Monks, F. Pop, E. S. Davies, R. C. I. MacKenzie, D. B. Amabilino, *Chem. Eur. J.* **2018**, *24*, 14461–14469.
[33] a) M. Kirkus, L. Wang, S. Mothy, D. Beljonne, J. Cornil, R. A. J. Janssen, S. C. J. Meskers, *J. Phys. Chem. A* **2012**, *116*, 7927–7936; b) T. He, P. Leowanawat, C. Burschka, V. Stepanenko, M. Stolte, F. Würthner, *Adv. Mater.* **2018**, *30*, 1804032.
[34] M. Boukhris, M. S. J. Simmonds, S. Sayadi, M. Bouaziz, *Phytother. Res.* **2013**, *27*, 1206–1213.
[35] a) P. Prasher, M. Sharma, *MedChemComm* **2019**, *10*, 1302–1328; b) L. da S. M. Forezi, C. G. S. Lima, A. A. P. Amaral, P. G. Ferreira, M. C. B. V. de Souza, A. C. Cunha, F. de C. da Silva, V. F. Ferreira, *Chem. Rec.* **2021**, *21*, 2782–2807; c) M. Serafini, T. Pirali, G. C. Tron in *Chapter Three: Click 1,2,3-Triazoles in Drug Discovery and Development: From the Flask to the Clinic? Vol. 134* (Eds.: N. A. Meanwell, M. L. Lolli), Academic Press, San Diego, **2021**, pp. 101–148; d) L. A. Aronica, G. Albano, *Catalysts* **2022**, *12*, 68.
[36] a) M. A. Naik, N. Venkatramaiah, C. Kanimozhi, S. Patil, *J. Phys. Chem. C* **2012**, *116*, 26128–26137; b) C. Kanimozhi, N. Yaacobi-Gross, E. K. Burnett, A. L. Briseno, T. D. Anthopoulos, U. Salzner, S. Patil, *Phys. Chem. Chem. Phys.* **2014**, *16*, 17253–17265; c) A. Ardizzone, D. Blasi, D. Vona, A. Rosspeintner, A. Punzi, E. Altamura, N. Grimaldi, S. Sala, E. Vauthey, G. M. Farinola, I. Ratera, N. Ventosa, J. Veciana, *Chem. Eur. J.* **2018**, *24*, 11386–11392; d) A. Punzi, D. Blasi, A. Operamolla, R. Comparelli, G. Palazzo, G. M. Farinola, *RSC Adv.* **2021**, *11*, 11536–11540.
[37] a) J. David, M. Weiter, M. Vala, J. Vyňuchal, J. Kučerík, *Dyes Pigm.* **2011**, *89*, 137–143; b) J. Lucarelli, M. Lessi, C. Manzini, P. Minei, F. Bellina, A. Pucci, *Dyes Pigm.* **2016**, *135*, 154–162; c) A. Punzi, E. Maiorano, F. Nicoletta, D. Blasi, A. Ardizzone, N. Ventosa, I. Ratera, J. Veciana, G. M. Farinola, *Eur. J. Org. Chem.* **2016**, *2016*, 2617–2627; d) M. Stolte, S.-L. Suraru, P. Diemer, T. He, C. Burschka, U. Zschieschang, H. Klauk, F. Würthner, *Adv. Funct. Mater.* **2016**, *26*, 7415–7422.
[38] a) J. Mei, K. R. Graham, R. Stalder, S. P. Tiwari, H. Cheun, J. Shim, M. Yoshio, C. Nuckolls, B. Kippelen, R. K. Castellano, J. R. Reynolds, *Chem. Mater.* **2011**, *23*, 2285–2288; b) C. Kanimozhi, N. Yaacobi-Gross, K. W.

Chou, A. Amassian, T. D. Anthopoulos, S. Patil, *J. Am. Chem. Soc.* **2012**, *134*, 16532–16535.
[39] W.-H. Chang, J. Gao, L. Dou, C.-C. Chen, Y. Liu, Y. Yang, *Adv. Energy Mater.* **2014**, *4*, 1300864.
[40] a) H. Ftouni, F. Bolze, J.-F. Nicoud, *Dyes Pigm.* **2013**, *97*, 77–83; b) G. Zhang, H. Li, S. Bi, L. Song, Y. Lu, L. Zhang, J. Yu, L. Wang, *Analyst* **2013**, *138*, 6163–6170; c) J. Schmitt, V. Heitz, A. Sour, F. Bolze, H. Ftouni, J.-F. Nicoud, L. Flamigni, B. Ventura, *Angew. Chem. Int. Ed.* **2015**, *54*, 169–173; *Angew. Chem.* **2015**, *127*, 171–175.
[41] a) K. E. Krakowiak, J. S. Bradshaw, *Synth. Commun.* **1996**, *26*, 3999–4004; b) I. Maqueira-Albo, G. Ernesto Bonacchini, G. Dell'Erba, G. Pace, M. Sassi, M. Rooney, R. Resel, L. Beverina, M. Caironi, *J. Mater. Chem. C* **2017**, *5*, 11522–11531; c) M. Shaker, B. Park, J.-H. Lee, W. Kim, C. K. Trinh, H.-J. Lee, J. W. Choi, H. Kim, K. Lee, J.-S. Lee, *RSC Adv.* **2017**, *7*, 16302–16310; d) J. H. L. Ngai, X. Gao, P. Kumar, J. Polena, Y. Li, *Adv. Electron. Mater.* **2021**, *7*, 2000935.
[42] a) D. S. Pal, S. Ghosh, *Chem. Eur. J.* **2018**, *24*, 8519–8523; b) D. S. Pal, H. Kar, S. Ghosh, *Chem. Commun.* **2018**, *54*, 928–931.
[43] a) A. Tamayo, T. Kent, M. Tantitiwat, M. A. Dante, J. Rogers, T.-Q. Nguyen, *Energy Environ. Sci.* **2009**, *2*, 1180–1186; b) M. E. Farahat, H.-Y. Wei, M. A. Ibrahem, K. M. Boopathi, K.-H. Wei, C.-W. Chu, *RSC Adv.* **2014**, *4*, 9401–9411; c) D. Yang, F. Cheng, J. Zhang, H. Li, *Thin Solid Films* **2018**, *645*, 209–214.
[44] a) Q. Chu, Y. Pang, *Macromolecules* **2003**, *36*, 4614–4618; b) R.-H. Chien, C.-T. Lai, J.-L. Hong, *J. Phys. Chem. C* **2011**, *115*, 5958–5965.
[45] a) G. Albano, M. Górecki, G. Pescitelli, L. Di Bari, T. Jávorfi, R. Hussain, G. Siligardi, *New J. Chem.* **2019**, *43*, 14584–14593; b) G. Albano, M. Górecki, T. Jávorfi, R. Hussain, G. Siligardi, G. Pescitelli, L. Di Bari, *Aggregate* **2022**, *3*, e193.
[46] a) G. Albano, G. Pescitelli, L. Di Bari, *Chem. Rev.* **2020**, *120*, 10145–10243; b) G. Albano, G. Pescitelli, L. Di Bari, *ChemNanoMat* **2022**, *8*, e202200219.
[47] a) J. Wade, J. N. Hilfiker, J. R. Brandt, L. Liirò-Peluso, L. Wan, X. Shi, F. Salerno, S. T. J. Ryan, S. Schöche, O. Arteaga, T. Jávorfi, G. Siligardi, C. Wang, D. B. Amabilino, P. H. Beton, A. J. Campbell, M. J. Fuchter, *Nat. Commun.* **2020**, *11*, 6137; b) B. Laidlaw, J. Eng, J. Wade, X. Shi, F. Salerno, M. J. Fuchter, T. J. Penfold, *Chem. Commun.* **2021**, *57*, 9914–9917.
[48] A. B. Tamayo, M. Tantiwiwat, B. Walker, T.-Q. Nguyen, *J. Phys. Chem. C* **2008**, *112*, 15543–15552.
[49] H. Zhan, Q. Liu, S.-K. So, W.-Y. Wong, *J. Organomet. Chem.* **2019**, *894*, 1–9.
[50] C. M. Cardona, W. Li, A. E. Kaifer, D. Stockdale, G. C. Bazan, *Adv. Mater.* **2011**, *23*, 2367–2371.

Manuscript received: January 27, 2023
Accepted manuscript online: March 23, 2023
Version of record online: ■■, ■■

RESEARCH ARTICLE

The impact of achiral substituents on the chiral supramolecular aggregation of diketopyrrolo[3,4-*c*]pyrrole-1,2,3-1*H*-triazole dyes is discussed here, giving special emphasis to ECD measurements.

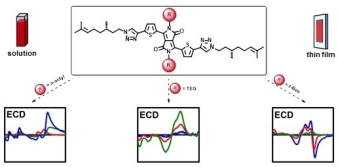

Dr. G. Albano, Dr. F. Zinna, A. Taddeucci, Prof. M. A. M. Capozzi, Prof. G. Pescitelli, Prof. A. Punzi, Prof. L. Di Bari*, Prof. G. M. Farinola*

1 – 17

Chiral Diketopyrrolo[3,4-*c*]pyrrole-1,2,3-1*H*-triazole Dyes with Highly Tuneable Properties in Solution and Thin Films